BNL-66927

JOURNAL OF GEOPHYSICAL RESEARCH, VOL. 105, NO. D1, PAGES 1387–1415, JANUARY 20, 2000

Sulfur chemistry in the National Center for Atmospheric Research Community Climate Model: Description, evaluation, features, and sensitivity to aqueous chemistry

M. C. Barth, P. J. Rasch, and J. T. Kiehl

National Center for Atmospheric Research, Boulder, Colorado

C. M. Benkovitz and S. E. Schwartz

Brookhaven National Laboratory, Upton, New York

Abstract. Sulfur chemistry has been incorporated in the National Center for Atmospheric Research Community Climate Model in an internally consistent manner with other parameterizations in the model. The model predicts mixing ratios of dimethylsulfide (DMS), SO_2, SO_4^{2-}, H_2O_2. Processes that control the mixing ratio of these species include the emissions of DMS and SO_2, transport of each species, gas- and aqueous-phase chemistry, wet deposition, and dry deposition of species. Modeled concentrations agree quite well with observations for DMS and H_2O_2, fairly well for SO_2, and not as well for SO_4^{2-}. The modeled SO_4^{2-} tends to underestimate observed SO_4^{2-} at the surface and overestimate observations in the upper troposphere. The SO_2 and SO_4^{2-} species were tagged according to the chemical production pathway and whether the sulfur was of anthropogenic or biogenic origin. Although aqueous-phase reactions in cloud accounted for 81% of the sulfate production rate, only ~50-60% of the sulfate burden in the troposphere was derived from cloud chemistry. Because cloud chemistry is an important source of sulfate in the troposphere, the importance of H_2O_2 concentrations and pH values was investigated. When prescribing H_2O_2 concentrations to clear-sky values instead of predicting H_2O_2, the global-averaged, annual-averaged in-cloud production of sulfate increased. Setting the pH of the drops to 4.5 also increased the in-cloud production of sulfate. In both sensitivity simulations, the increased in-cloud production of sulfate decreased the burden of sulfate because less SO_2 was available for gas-phase conversion, which contributes more efficiently to the tropospheric sulfate burden than does aqueous-phase conversion.

1. Introduction

Understanding the tropospheric sulfur cycle is important because of its contribution to acid rain and its effect on the Earth's radiation balance. The role of sulfuric acid in acid rain has been recognized for well over a hundred years [see *Cowling*, 1982], but the role of sulfate aerosols on the Earth's climate has been recognized only somewhat more recently [*Twomey*, 1977, *Charlson et al.*, 1987, 1991]. Sulfate aerosols can directly influence the atmospheric radiation budget by scattering solar radiation. The sulfate aerosols also can indirectly affect the radiation budget through their modification of cloud properties. Sulfate aerosols are a source of cloud condensation nuclei (CCN), and when there are more CCN, more cloud drops are formed thus increasing the albedo and lifetime of the cloud [*Albrecht*, 1989]. Evidence for the indirect effect has been noted in studies of ship tracks [*Radke*, 1988, *Coakley et al.* 1988]. There has also been evidence of the indirect effect in remote regions of the world. *Hegg et al.* [1991a, b] showed correlations of dimethylsulfide (DMS) mixing ratios with CCN and cloud droplet concentrations in the northeast Pacific Ocean. In the Southern Hemisphere, *Boers et al.* [1994] showed a relation between the optical depth of clouds derived from satellite and boundary layer CCN concentrations over a 10-year period. This extensive period allowed seasonal variations of DMS mixing ratios, CCN concentrations, and cloud optical depth to illustrate higher values of these variables in summer when

Copyright 2000 by the American Geophysical Union.

Paper number 1999JD900773.
0148-0227/00/1999JD900773$09.00

warmer temperatures and higher DMS fluxes occur and lower values in winter.

Numerical models of tropospheric sulfur chemistry have been used on the mesoscale to examine the cloud chemistry that creates sulfate [e.g. *Tremblay and Leighton*, 1986, *Hegg et al.*, 1989; *Chaumerliac et al.*, 1987] on the regional scale to examine acid deposition [*Chang et al.*, 1987, *Venkatram et al.*, 1988; *Carmichael et al.*, 1986] and recently on the subhemispheric to global scale to examine the effect of aerosols on climate [*Langner and Rodhe*, 1991, *Taylor and Penner*, 1994; *Benkovitz et al.*, 1994; *Pham et al.*, 1995; *Feichter et al.*, 1996; *Chin et al.*, 1996; *Kasibhatla et al.*, 1997; *Roelofs et al.*, 1998]. There have been several improvements in the depiction of the processes contributing to sulfate production since the pioneer work of *Langner and Rodhe* [1991]. The models have increased the spatial and temporal resolution, have included better parameterizations of clouds [*Feichter et al.*, 1996], and have better descriptions of gas-phase reactions [*Pham et al.*, 1995, *Chin et al.*, 1996; *Roelofs et al.*, 1998], aqueous-phase reactions [*Feichter et al.*, 1996, *Roelofs et al.*, 1998], wet deposition of sulfur species [*Chin et al.*, 1996, *Feichter et al.*, 1996]; and dry deposition [*Chin et al.*, 1996, *Kasibhatla et al.*, 1997; *Roelofs et al.*, 1998]. This study presents results from a three dimensional global sulfur model that is embedded in the National Center for Atmospheric Research (NCAR) Community Climate Model (CCM). The model described here includes a state of the art climate model, prediction of hydrogen peroxide (H_2O_2) concentrations in addition to DMS, sulfur dioxide (SO_2), and aerosol sulfate (SO_4^{2-}), and a wet deposition scheme that is based upon local abundances of a species and the flux of that species downward via precipitation.

The NCAR global sulfur model has been used to examine the influence of sulfate aerosols on the atmospheric radiation budget [*Kiehl et al.*, 1999] and to describe the processes that control the aerosol sulfate burden [*Rasch et al.*, this issue]. Here we present an in-depth description of the global sulfur model, an illustration of results from a 6-year simulation, an evaluation of the accuracy of these results, and an examination of the influence of cloud chemistry on the aerosol sulfate burden.

2. Model Description

The model in which the sulfur chemistry is embedded is the NCAR Community Climate Model, Version 3 (CCM3). The CCM3 [*Kiehl et al.*, 1998] was configured to a T42 grid (2.8° × 2.8° horizontal resolution), 18 vertical levels, which are set on a hybrid-sigma coordinate, from the surface to the 5 hPa height, and a centered time step of 20 min. The CCM3 transports water vapor, chemical species, and temperature consistently via a semi-Lagrangian advection scheme, a penetrative convection scheme, and a nonlocal planetary boundary layer transport scheme with a countergradient term. The cloud fraction in CCM3 is a function of the relative humidity, stability, and vertical velocity. The radiation code distinguishes cloud particle size by phase and location, where the cloud water drop size is 5 μm over land and 10 μm over ocean, the cloud ice crystal size is between 10 and 30 μm, and the aerosol optical depth is set to 0.14 uniformly over the Earth. In the version of CCM3 used for this study a prognostic cloud water scheme was employed [*Rasch and Kristjánsson*, 1998] that assumes the cloud drop concentration over land at low altitudes to be 400 cm^{-3} and the cloud drop concentration over the ocean and at high altitudes to be 80 cm^{-3}.

The sulfur chemistry represented in the model includes emissions, transport, gas and aqueous reactions, and wet and dry deposition of dimethylsulfide, sulfur dioxide, aerosol sulfate, and hydrogen peroxide. The sulfate aerosols do not interact with other physical processes depicted in the CCM; thus the aerosol-climate feedback is not described by these simulations but rather is diagnosed from the model results [*Kiehl et al.*, 1999]. Transport processes of trace gases and aerosols include resolved-scale advection and subgrid-scale convection and diffusion. The convection in CCM3 is treated using two parameterizations. The *Zhang and McFarlane* [1995] parameterization uses bulk plumes with entrainment and detrainment for the updrafts and downdrafts that are intended to represent an ensemble of deep convective elements. The *Hack* [1994] parameterization represents primarily shallow trade cumuli. Both parameterizations transport moisture, heat, and trace species in an internally consistent fashion. The convective transport of trace gases and aerosols is performed on the interstitial fraction of these species in the cloudy volume and the fraction of dissolved material in the cloud drops that do not undergo microphysical transformation to precipitation. The gases and aerosols inside the cloud drops can be detrained at higher levels in the model. The processes are calculated using operator splitting from the $n-1$ to $n+1$ time level (i.e., a 40-min time step), except for the aqueous chemistry, which uses a 2-min time step during each 40-min interval.

2.1. Emissions

Emissions of sulfur species in the model include anthropogenic emissions of SO_2 and SO_4^{2-} and oceanic emissions of DMS; volcanic and biomass burning sources currently are excluded. Anthropogenic emissions were obtained from the Global Emissions Inventory Activity (GEIA) emissions inventory [*Benkovitz et al.*, 1996], which is representative of 1985 emissions. The seasonally averaged emissions data were provided at the surface and at 100 m and above to accomodate emissions from industry stacks (Plate 1). The anthropogenic emissions, whose total global emission rate was 67 Tg S yr^{-1}, were assumed to be 98% by mole SO_2 and 2%

SO_4^{2-}. Since the emissions inventory supplied data at two levels and the height of the interface between the bottom two model levels was generally above 100 m (average height was ~120 m), we apportioned a fraction of the emissions data from above 100 m to the bottom level of the model. The fraction into the bottom level was determined as

$$\frac{zi(1) - 100}{zi(2) - 100},$$

where $zi(1)$ is the height of the top of the lowest level of the model and $zi(2)$ is the height of the top of the second lowest level of the model.

The emissions of DMS were obtained from the biogenic sulfur emissions inventory compiled at Brookhaven National Laboratory that was based on the methodology used by *Benkovitz et al.* [1994]. This method derived sulfur emissions in latitude bands from the work of *Bates et al.* [1992] and distributed the emissions across the latitude band according to ocean color using the Coastal Zone Color Scanner. DMS emissions were obtained from the biogenic emissions data by choosing biogenic emissions only from the oceans (Plate 1). The global emission rate from DMS was 15.5 Tg S yr^{-1}.

2.2. Gas-Phase Reactions

Oxidation of SO_2 to form sulfate, oxidation of DMS to form SO_2, and production and destruction of H_2O_2 are represented in the model (Table 1). In R1, it is assumed that the SO_2 + OH reaction is the rate-limiting step of the multistep process of forming aerosol sulfate. Concentrations of short-lived radicals OH, NO_3, and HO_2 are prescribed using three-dimensional, monthly averaged concentrations obtained from the Intermediate Model of Global Evolution of Species (IMAGES) [*Müller and Brasseur*, 1995]. The diurnal variation of these oxidants is not included in our calculations, but instead, the diurnally averaged value is used at each time step. The rate coefficient for (R2) follows *Benkovitz et al.* [1994], who followed the work of *Yin et al.* [1990a, b]. The rate of H_2O_2 photolysis is determined via a look-up table method where the photolysis rate depends on the diurnally averaged zenith angle and the height of the gridpoint, assuming that the albedo for ul-

Table 1. Reactions Included in the Global Sulfur Model

				k_{298}[a]	$\frac{E}{R}$	Reference[b]
			Gas Chemistry			
(R1)	$SO_2 + OH + M$	→	$SO_4^{2-} + M$	$k_o = 3.0\times 10^{-31}(\frac{T}{300})^{-3.3}$ $k_\infty = 1.5\times 10^{-12}$		NASA97
(R2)	DMS + OH	→	$\alpha SO_2 + (1 - \alpha)$ MSA [c]			Y90
(R3)	$DMS + NO_3$	→	$SO_2 + HNO_3$	1.0×10^{-12}	500.	NASA97
(R4)	$HO_2 + HO_2$	→	$H_2O_2 + O_2$	8.6×10^{-12}	-590.	NASA97
(R5)	$H_2O_2 + h\nu$	→	2OH	see text		
(R6)	$H_2O_2 + OH$	→	$HO_2 + H_2O$	1.7×10^{-12}	160.	NASA97
			Aqueous Chemistry			
(R7)	$HSO_3^- + H_2O_2$	→	$SO_4^{2-} + 2H^+ + H_2O$	2.7×10^7 [d]	4750.	HC85
(R8)	$HSO_3^- + O_3$	→	$SO_4^{2-} + H^+ + O_2$	3.7×10^5	5300.	HC85
(R9)	$SO_3^{2-} + O_3$	→	$SO_4^{2-} + O_2$	1.5×10^9	5280.	HC85
			Equilibrium Reactions			
(R10)	H_2O_2 (g)	⇌	H_2O_2 (aq)	7.4×10^4	-6621.	LK86
(R11)	O_3 (g)	⇌	O_3 (aq)	1.15×10^{-2}	-2560.	NBS65
(R12)	SO_2 (g)	⇌	SO_2 (aq)	1.23	-3120.	NBS65
(R13)	H_2SO_3	⇌	$HSO_3^- + H^+$	1.3×10^{-2}	-2015.	M82
(R14)	HSO_3^-	⇌	$SO_3^{2-} + H^+$	6.3×10^{-8}	-1505.	M82

[a]Units for first order reactions are s^{-1}, for the second-order gas reactions are $molecules^{-1}\ cm^3\ s^{-1}$, for the third-order gas reactions $molecules^{-2}\ cm^6\ s^{-1}$, and for the second-order aqueous reactions are $M^{-1}\ s^{-1}$. Units for solubility constants are M atm^{-1}, and units for dissociation constants are M. Reaction rates are of the form $k = k_{298}\exp[-\frac{E}{R}(\frac{1}{T} - \frac{1}{298})]$ unless otherwise noted.

[b]NASA97, *Demore et al.* [1997]; Y90, *Yin et al.* [1990a, b]; HC85, *Hoffmann and Calvert* [1985]; LK86, *Lind and Kok* [1986]; NBS65, *National Bureau of Standards* [1965]; and M82, *Maahs* [1982].

[c]Here $k = \frac{Te^{-234/T} + 8.46\times 10^{-10}e^{7230/T} + 2.68\times 10^{-10}e^{7810/T}}{1.04\times 10^{11}T + 88.1e^{7460/T}}$.

[d]Here $k = \frac{k_{298}\exp[-\frac{E}{R}(\frac{1}{T} - \frac{1}{298})][H^+]}{1 + 13[H^+]}$.

traviolet radiation is 0.3. Because R4 is nonlinear and the diurnally averaged rate of reaction does not equal the reaction rate of diurnally averaged HO_2 mixing ratios, the HO_2 mixing ratios are adjusted by the amount of daylight at any given latitude. The rates of the sulfur reactions are determined by the effective first-order rate coefficient and using a quasi-steady state approximation [*Hesstvedt et al.*, 1978]. The H_2O_2 concentration determined from the gas-phase reactions is calculated using an Euler forward approximation.

2.3. Aqueous-Phase Reactions

Oxidation of aqueous SO_2 by O_3 and H_2O_2 to form SO_4^{2-}
aerosol is included in the model (Table 1). The concentrations of O_3 are prescribed using three-dimensional, monthly averaged concentrations obtained from the IMAGES model. The pH of the drops is determined diagnostically assuming an NH_4^+ to SO_4^{2-} molar ratio of 1.0.

$$[H^+] = [HSO_3^-] + [SO_4^{2-}].$$

The liquid water content in a grid cell is determined by combining the resolved-scale cloud water mixing ratio that is predicted, the subgrid-scale deep convective and shallow convective cloud water mixing ratios, and the resolved-scale rain mixing ratio that is diagnosed from the precipitation rate using a mass-weighted fall speed, which is determined assuming a *Marshall and Palmer* [1948] size distribution of rain. SO_2 and H_2O_2 are depleted and SO_4^{2-} is produced only in the cloudy region of the grid box. The grid box concentration of these species is found by multiplying the cloudy region concentration times the cloud fraction and the clear air concentration times the fraction of clear air in the grid box.

Because the rate of S(IV) (= $SO_2 \cdot H_2O + HSO_3^- + SO_3^{2-}$) oxidation by O_3 depends on the pH of the drops, the aqueous-phase reactions are evaluated using a 2-min time step with an Euler forward numerical approximation. At the end of each 2-min time step the hydrogen ion concentration is recalculated so that the influence of pH on S(IV) oxidation is captured. *Feichter et al.* [1996] used a similar method.

2.4. Wet Deposition

The wet deposition rates are calculated separately for gases and aerosols. Cloud water and rain mixing ratios from both the resolved clouds and the subgrid-scale clouds are determined for the cloudy volume in each grid column. For temperatures between -20° and 0°C the cloudy fraction is a mixture of liquid and ice, where the ice and cloud water mixing ratios are determined by a linear fit between these two temperatures. At temperatures below -20°C, only cloud ice exists, and at temperatures above 0°C, only the liquid phase exists. For temperatures below 0°C the precipitation is assumed to be all snow; otherwise, it is assumed to be rain. Trace gases are scavenged only by the liquid hydrometeors, whereas aerosols can also be scavenged by snow.

The fraction of a trace gas that is in the liquid water is determined through each species' Henry's law coefficient, which is temperature- and/or pH-dependent. At any particular level in the model the flux of the dissolved trace gas in the precipitation entering the grid cell from above is found. The trace gas is reequilibrated with the current model level's properties. Then the flux of the dissolved trace gas exiting the model level is determined. The rate of wet deposition is found from the flux divergence, maintaining mass conservation.

The wet deposition of aerosols is performed in a similar flux method. Any layer in the model can undergo both below-cloud and in-cloud scavenging. The below-cloud scavenging follows *Dana and Hales* [1976] and *Balkanski et al.* [1993]. It is assumed that both rain and snow, which has graupel-like characteristics (and therefore characteristics similar to rain), scavenge the aerosol below cloud. Removal is assumed to take place by a first-order loss process. That is,

$$L_{W,bc} = 0.1Pq$$

where $L_{W,bc}$ is the loss rate by below-cloud scavenging, 0.1 is the collection efficiency, P is the precipitation flux expressed in mm h^{-1}, and q is the species mass mixing ratio. For in-cloud scavenging in stratiform clouds (resolved by the model), 100% of the aerosol mass is assumed to reside in the cloud water and rain. The fraction of cloud water that is converted to rain through coalescence and accretion processes has a proportionate amount of sulfate aerosol transferred to the precipitation. This fraction of the aerosol is removed through wet deposition. Wet deposition of aerosols in convective clouds is determined similarly to the stratiform cloud scavenging. Evaporation of rain is accounted for in the wet deposition rate calculation by releasing a proportionate mass of aerosol to the atmosphere (i.e., if 10% of the precipitation evaporates, then 10% of the sulfate aerosol is released back to the air). This last assumption could lead to an overestimate of sulfate mixing ratios in the air [*Barth et al.*, 1992] because the number of drops that completely evaporate (and therefore the amount of sulfate aerosol released from the drop to the air) is not necessarily proportional to the mass of rain that evaporates.

2.5. Dry Deposition

Calculation of dry deposition rates follows that described by *Benkovitz et al.* [1994]. The deposition velocity of SO_2 is determined following the series resistance method outlined by *Wesely* [1989] where the deposition velocity is inversely proportional to the sum of the aerodynamic resistance, the resistance to transport across the atmospheric sublayer in contact with surface elements, and the surface resistance. The aerodynamic

and sublayer resistances are determined using boundary layer meteorological parameters. The surface resistance is found through a parameterization outlined by *Wesely* [1989]. Data needed for these calculations include land use classifications derived from *Wilson and Henderson-Sellers* [1985], boundary layer meteorological parameters obtained from the boundary layer parameterization in the CCM, surface roughness, and resistances for various land use types given by *Wesely* [1989]. The deposition velocity of aerosol sulfate is calculated in the same manner as *Benkovitz et al.* [1994] and is based on the inverse of the sum of the aerodynamic and sublayer resistances, which depend on micrometeorological parameters.

2.6. Initial Conditions and Order of Calculations

Initially mixing ratios of all the trace species (SO_2, SO_4^{2-}, DMS, and H_2O_2) are set to zero. Prescribed species (O_3, OH, HO_2, and NO_3) are set according to the linearly interpolated concentration for the location of the grid point and the time of year.

The order of the chemistry calculations is as follows. The aqueous chemistry is performed after the cloud water mixing ratio is determined. The new H_2O_2, SO_2, and SO_4^{2-} concentrations are then used for the gas chemistry calculations. The modified H_2O_2, SO_2, and SO_4^{2-} concentrations then are used in the wet deposition calculation. To reduce any bias introduced by having the aqueous and gas chemistry calculations occur before the wet deposition calculation, a toggle was placed into the code to alternate the order between the aqueous plus gas chemistry and the wet deposition calculations. After the chemistry and wet deposition are calculated, transport through subgrid convective cores is determined for the interstitial fraction of each species (because of their high solubility, sulfate aerosols are not convectively transported). Because a centered time step is used, a time filter couples the concentrations from the odd and even time step integrations. Then the emissions and dry deposition calculations are performed.

3. Results

The base simulation, presented in this paper, which used present-day (1985) emissions, tagged the sulfate and SO_2 species according to the chemical production pathway and whether the sulfur was biogenic or anthropogenic in origin. Other simulations included tagging the SO_2 and SO_4^{2-} by region [*Rasch et al.*, this issue] and a base simulation that used preindustrial emissions [*Kiehl et al.*, 1999].

The base simulation was integrated for 6 years; a quasi-equilibrium was found from year 2 onward [*Rasch et al.*, this issue]. Results described in this paper are average values of years 3–6 of the simulation. However, because the sensitivity simulations presented in section 6 and by *Rasch et al.* [this issue] and *Kiehl et al.* [1999] illustrate results from just 1 year, year 3 of the simulation, model results of year 3 are also compared to monthly mean surface observations and aircraft observations. This way the discussion of the sensitivity simulations can be evaluated with the observations.

Plate 1 illustrates the annual mean sulfur emissions and annual mean column burdens of SO_2, DMS, and SO_4^{2-}. The SO_2 emissions indicate that more SO_2 is emitted above 100 m than at the surface and that the emissions are patchy. The SO_2 column burden shows that the SO_2 remains close to the emission regions but also shows SO_2 plumes downwind of the emission regions. DMS emissions are also patchy, with the largest emissions occurring in upwelling regions and the southern oceans. The emissions of DMS are 20% of the SO_2 emissions. The column burden of DMS reflects its emission pattern and is much smaller than the SO_2 and SO_4^{2-} column burden. The SO_4^{2-} column burden shows that the greatest amounts of SO_4^{2-} occur near the anthropogenic sources but also shows SO_4^{2-} residing throughout the Northern Hemisphere.

Vertical distributions of the annual average, zonal average mixing ratios of SO_4^{2-}, SO_2, H_2O_2, and DMS are shown in Figure 1. Sulfate exhibits large concentrations in the Northern Hemisphere, as expected, but also significant concentrations in the tropics, which are vertically fairly homogeneous. This is in contrast to previous work, which generally showed a depletion of SO_4^{2-} in the midtroposphere tropics [*Langner and Rodhe*, 1991, *Pham et al.*, 1995, *Feichter et al.*, 1996]. Differences between our results and these previous simulations likely occur because of differences in the parameterizations of convective transport and wet deposition of the precursor species between the models. A comparison of our results to *Feichter et al.* [1996] shows that SO_2 from our model is greater than SO_2 from *Feichter et al.* [1996] above the 400 hPa level and is less than SO_2 from *Feichter et al.* [1996] below the 700 hPa level, indicating different vertical transport schemes of partially soluble species. A large influence of Northern Hemisphere SO_2 is seen throughout the Northern Hemisphere troposphere and even reaching the tropical upper troposphere. The annual averaged, zonal averaged H_2O_2 mixing ratios are similar to those shown by *Chin et al.* [1996] and *Feichter et al.* [1996] and reflect the input mixing ratios of HO_2. The annual averaged, zonal averaged DMS mixing ratios show the largest values near the surface in the Southern Hemisphere. Because of the strong DMS source strength in the Southern Hemisphere, larger values of DMS occur in the Southern Hemisphere midtroposphere than in the Northern Hemisphere. It is evident that DMS is convectively pumped in the tropics where, in the DMS emissions inventory used for this study, relatively high amounts of DMS are emitted especially near the west coasts of South America and Africa.

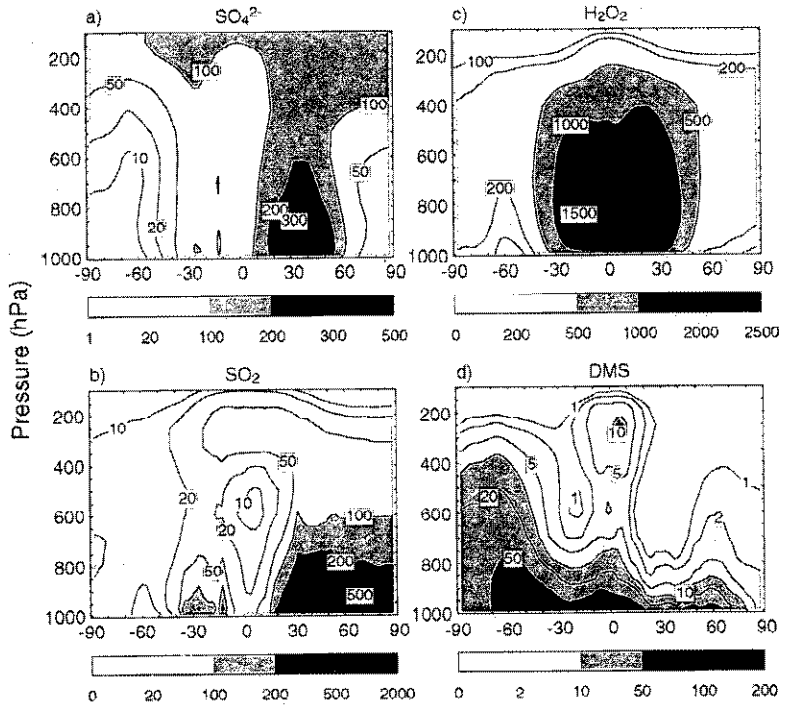

Figure 1. Zonal-averaged mixing ratios (pmol (mol air)$^{-1}$) of the annual-averaged (a) SO_4^{2-} (b) SO_2, (c) H_2O_2, and (d) DMS.

The distribution of sulfate aerosols varies quite a bit both temporally and spatially (Plate 2). Most of the variability occurs near source regions and downstream from these regions. This is especially true of Europe in July. The least amount of variability for these 2 months occurs in remote regions such as northeast of the North American continent in the Arctic, the equatorial regions near South America, and Antarctica.

4. Comparison With Observations

Departures from one-to-one agreement between model results and observations may arise both from model inaccuracies and from the fact that the comparison is done between climatologically driven model results and observations made at a certain location and time. The observations were obtained at surface stations, from balloon-borne aerosol sulfate concentrations, from aircraft field programs, and from satellite-borne measurements. SO_2 and SO_4^{2-} measurements from the surface stations include the European Monitoring and Evaluation Programme (EMEP) network in western Europe and the Eulerian Model Evaluation Field Study (EMEFS) network in the eastern United States. Other monitoring stations include locations in the Southern Hemisphere for DMS concentrations, locations primarily in the Northern Hemisphere industrial and Arctic regions for SO_2 concentrations, and locations worldwide for SO_4^{2-} concentrations. Observations from the monitoring and network stations capture the seasonal trends of trace species, but individual measurements could have local effects that are not captured in the context of a coarse-resolution global model. Furthermore, these stations do not provide the distribution of a species vertically. The balloon-borne measurements provide long-term observations of aerosols from the surface to the stratosphere but only at a single location, near Laramie, Wyoming, and without attribution to specific chemical composition. Model results are also compared to measurements from three Pacific Exploratory Mission (PEM) aircraft field programs, PEM-West A, PEM-West B, and PEM-Tropics A. These aircraft data provide a detailed distribution of the species both vertically and horizontally, but aircraft observations can only be made over a short period of time; thus it is never clear to what extent the measurements are representative of the region over a longer period of time. Finally, aerosol measurements from the Stratospheric Aerosol and Gas Experiment (SAGE) satellite give time and horizontal distributions, but again, the measurements provide no chemical identification. Also, the measurements are affected by the presence of clouds, which attenuate the signal; this can certainly be a problem in regions with frequent clouds such as the Intertropical Convergence Zone.

4.1. Network and Monitoring Stations

Similar to *Kasibhatla et al.* [1997], we have compared the Northern Hemisphere winter and summer average surface mixing ratios of SO_2 and non-sea-salt sulfate (nss-SO_4^{2-}) observed in North America [*McNaughton and Vet*, 1996] and western Europe for measurements

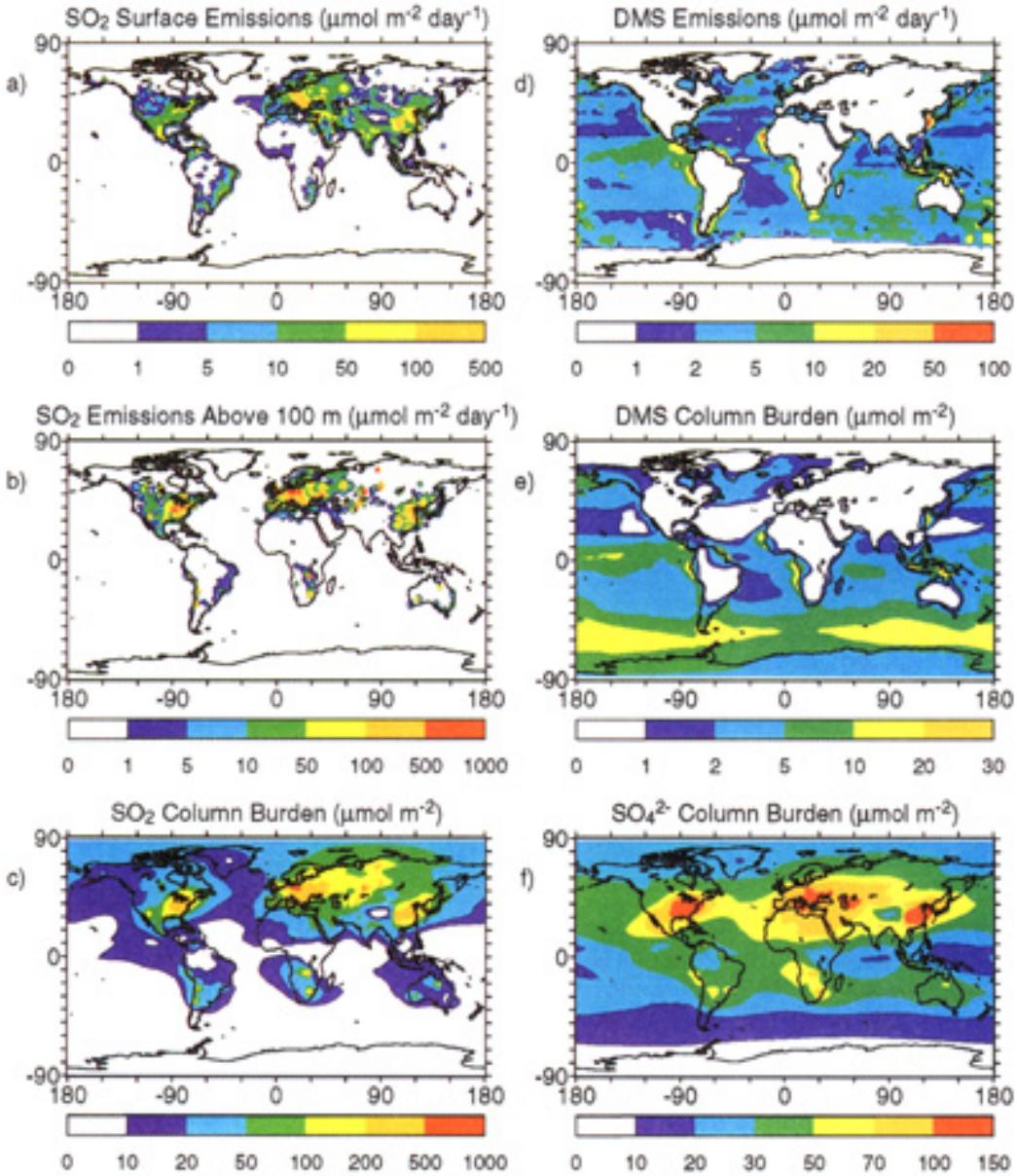

Plate 1. Annual-mean (a) SO_2 surface emissions, (b) SO_2 emissions above 100 m, (c) SO_2 column burden, (d) dimethylsulfide (DMS) emissions, (e) DMS column burden, and (f) sulfate column burden.

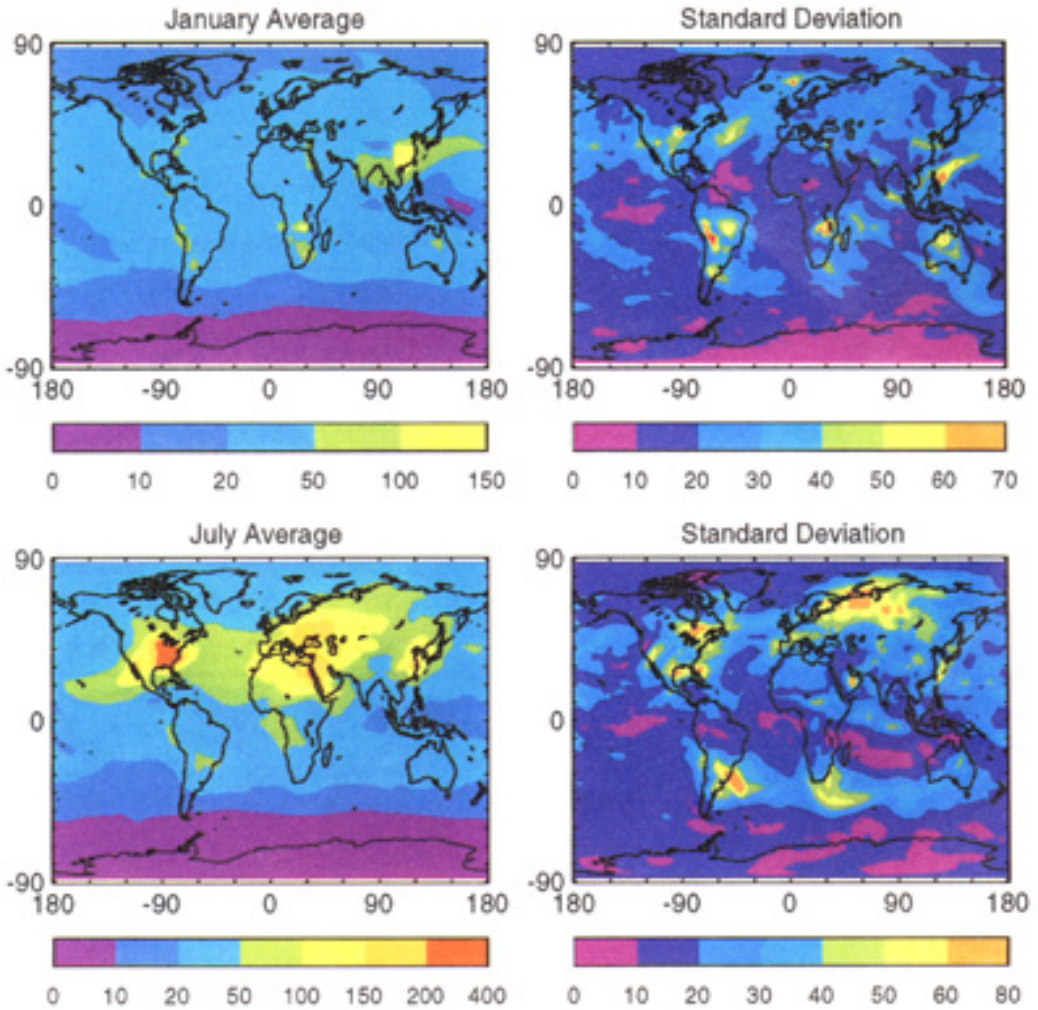

Plate 2. January and July average sulfate column burden (μmol m^{-2}) and standard deviation (%) of the daily burden relative to the monthly mean.

taken at surface stations below 500 m above mean sea level (msl) [*Schaug et al.*, 1987] to model results of years 3-6 in the model simulation. The data included near-daily measurements of SO_2 and SO_4^{2-} air concentrations, rainwater sulfate concentration, and precipitation from each region. The data were processed according to the procedure described by *Kasibhatla et al.* [1997] to a 265-km grid in each region. Figure 2 illustrates the location of each point used for comparison. Model results at the surface were interpolated to these locations. In both Europe and North America, modeled SO_2 concentrations agree with observations within a factor of 2 for both winter and summer seasons (Figure 3). However, modeled SO_4^{2-} concentrations are systematically lower than the observed concentrations in both regions. *Kasibhatla et al.* [1997] obtained similar results for these

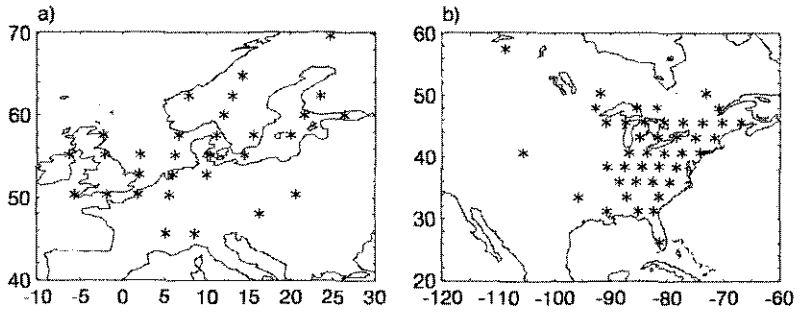

Figure 2. Location of points used for comparison from the network stations in (a) Europe and (b) eastern North America.

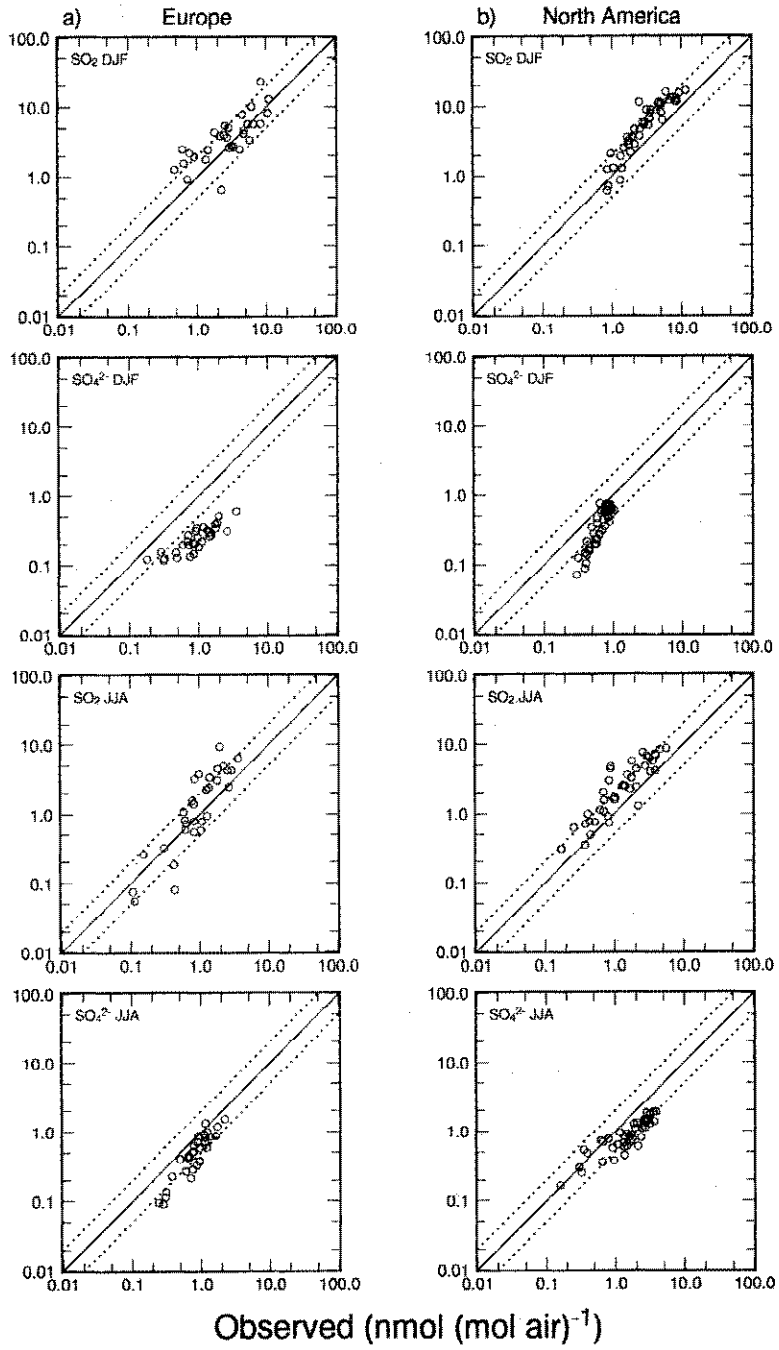

Figure 3. Observed versus modeled SO_2 and aerosol sulfate mixing ratios for winter and summer in (a) Europe and (b) eastern North America. Solid line denotes the one-to-one correspondence between model and observations; dotted lines denote a factor of 2 departure. Model results are for years 3–6 of the simulation. The data from the Eulerian Model Evaluation Field Study (EMEFS) network in North America were obtained from July 1988 to May 1990 [*McNaughton and Vet*, 1996]; the data from the European Monitoring and Evaluation Programme (EMEP) network in Europe were obtained from 1983 to 1992.

two industrial regions and seasons. The discrepancy between modeled and observed sulfate could be due to insufficient conversion of SO_2 to SO_4^{2-} predicted by the model, as SO_2 appears to be slightly overpredicted by the model, whereas SO_4^{2-} is underpredicted. The influence of the aqueous chemistry upon the sulfate burden is discussed in section 6. The measured wet deposition of SO_4^{2-} was determined from the near-daily measurements of rainwater SO_4^{2-} concentration and precipitation and was processed according to the procedure outlined by *Kasibhatla et al.* [1997]. Despite the disagreement between model and observations for aerosol sulfate concentrations the comparison of wet deposition rates of sulfur agree within a factor of 2 for both winter

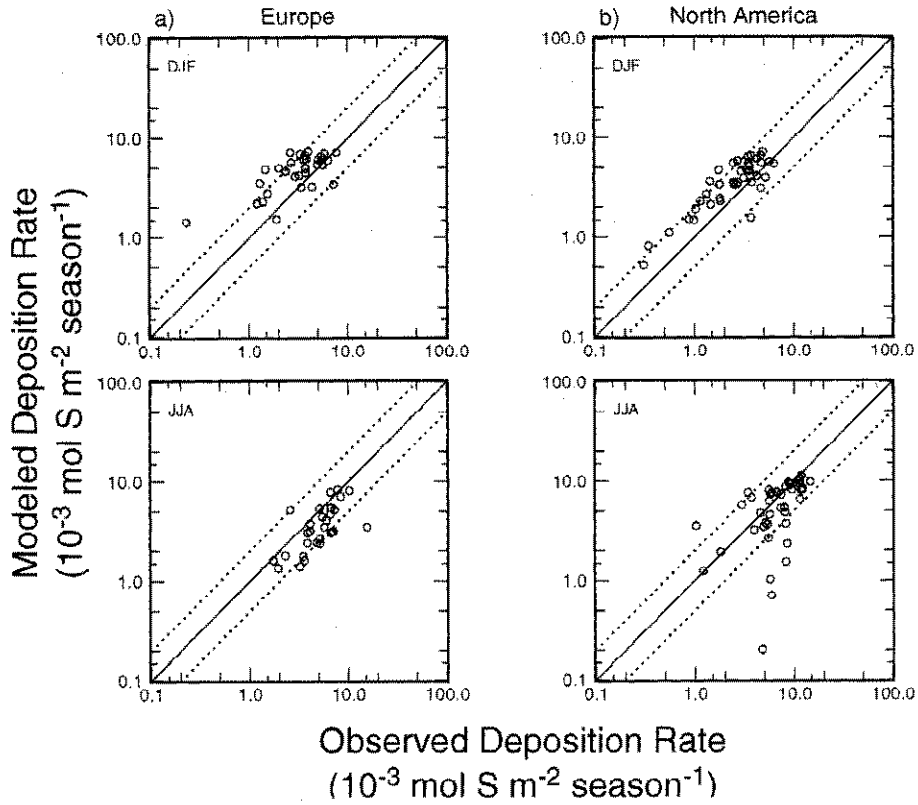

Figure 4. Observed versus modeled sulfur wet deposition rate for winter and summer in (a) Europe and (b) eastern North America. Solid line denotes the one-to-one correspondence between model and observations; dotted lines denote a factor of 2 departure. Model results are for years 3–6 of the simulation.

and summer in both regions except for eight sites in the eastern United States during summer (Figure 4).

Similar to *Chin et al.* [1996], we have compared model results to observations of DMS at remote monitoring stations (Figure 5). Modeled monthly mean DMS concentrations are higher than measured DMS (by as much as a factor of 5), but the modeled DMS exhibits a seasonal trend that is similar to the observed trend. The overprediction of DMS by the model may be due to uncertainties in the DMS emissions inventory, especially for the locations of these two monitoring stations, which are in high DMS emission regions. Another possible reason that DMS is overpredicted by the model at these two locations is that DMS could be reacting with atomic chlorine derived from methylhalides [*Keene et al.*, 1996], a reaction that is not represented in this model. The importance of these reactions has not sufficiently been tested, although *Chin et al.* [1996] obtained

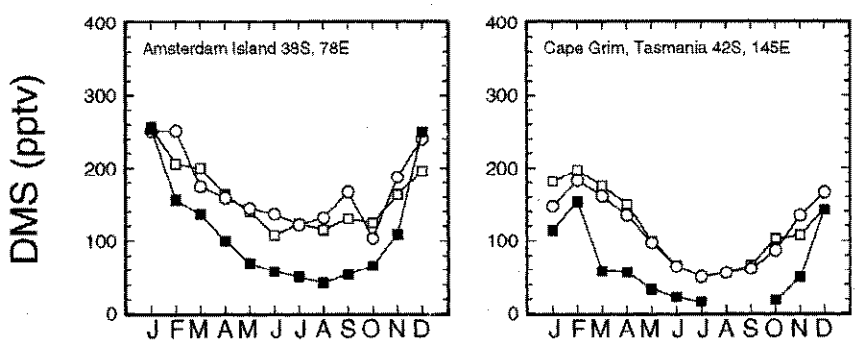

Figure 5. Monthly averaged DMS mixing ratio as a function of month at Amsterdam Island and Cape Grim. Open squares are the model results for years 3–6 of the simulation, open circles are the model results for year 3 of the simulation, and solid squares are the observations. Measurements of DMS were measured daily at Amsterdam Island [*Nguyen et al.*, 1992] for more than 4 years in the mid and late 1980s and were measured weekly at Cape Grim [*Ayers et al.*, 1991] from November 1988 to May 1990.

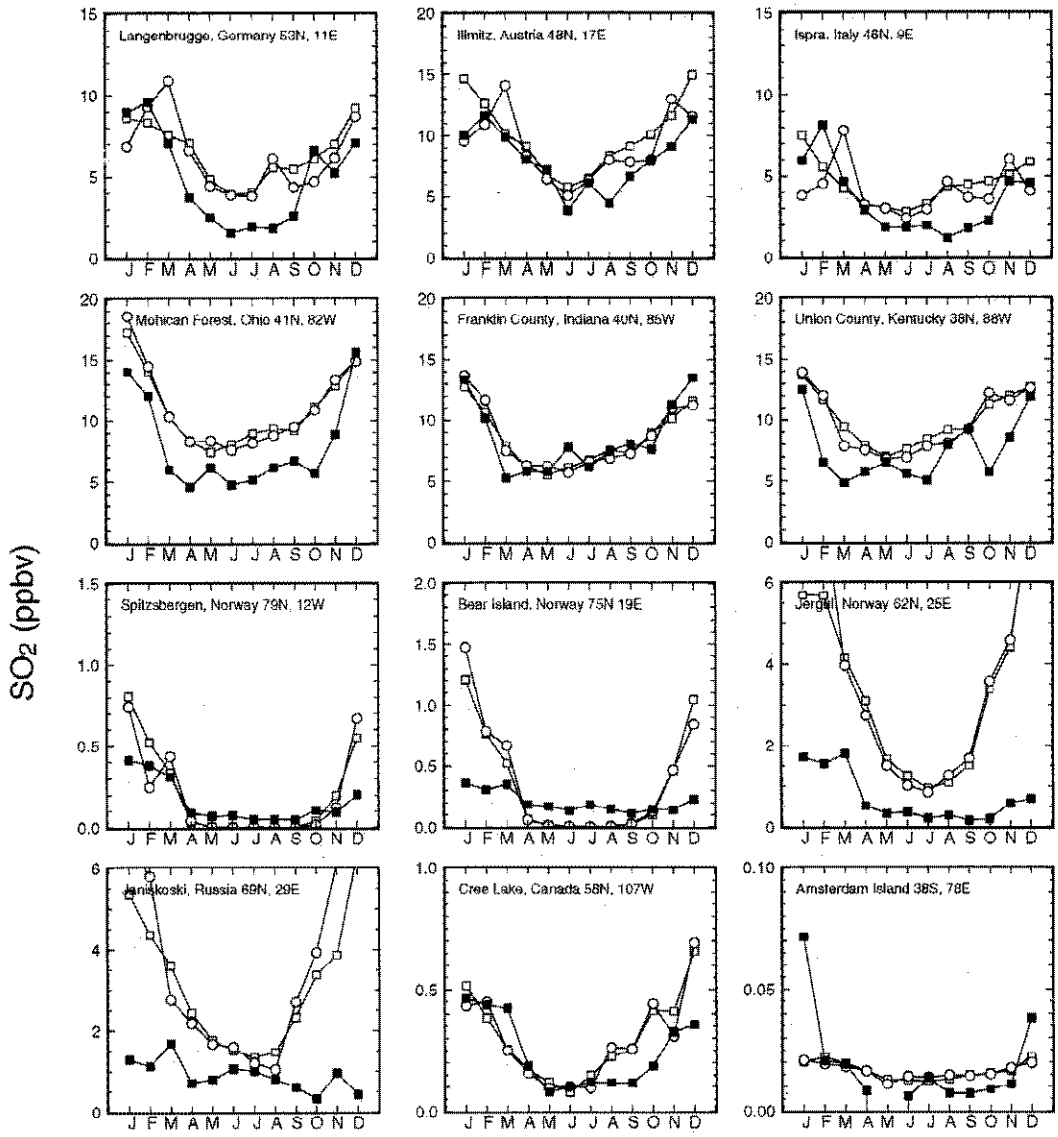

Figure 6. Monthly averaged SO_2 mixing ratio as a function of month at 12 different monitoring stations. Open squares are the model results for years 3–6 of the simulation, open circles are the model results for year 3 of the simulation, and solid squares are the observations. Measurements were obtained at EMEP locations from 1986 to 1992 [*Schaug et al.*, 1987], at sites in the United States from May 1980 to August 1981 [*Shaw and Paur*, 1983], at Cree Lake, Canada, from 1982 to 1988 [*Barrie and Bottenheim*, 1990], at Bear Island, Norway, from October 1978 to September 1981 [*Heintzenberg and Larssen*, 1983], and at Amsterdam Island from March 1989 to January 1991 [*Nguyen et al.*, 1992].

good agreement with observations when they employed an additional (unknown) chemical sink for DMS in their model.

SO_2 mixing ratios measured at locations in both remote and industrial regions are used to evaluate modeled SO_2 mixing ratios. In the northern midlatitudes the monthly mean SO_2 mixing ratios from the model agree well with the observations (Figure 6). However, for stations in Scandinavia and Canada the agreement between observations and model results is poorer. Generally, summertime values agree well, whereas in wintertime the model overpredicts the SO_2 mixing ratios. This suggests either that transport of SO_2 to the Arctic and Subarctic is too large or that the sinks of SO_2 are not properly captured for the Arctic and Subarctic. At Amsterdam Island, model results agree with observations during all the months except December and January, when the observations are much greater than the model results. When juxtaposed with the DMS measurements and model results at Amsterdam Island, it appears that the model predicts the correct amount of SO_2 when DMS is greater than observations and that the model predicts too little SO_2 when DMS is the same as observations. If the model is accurately depicting

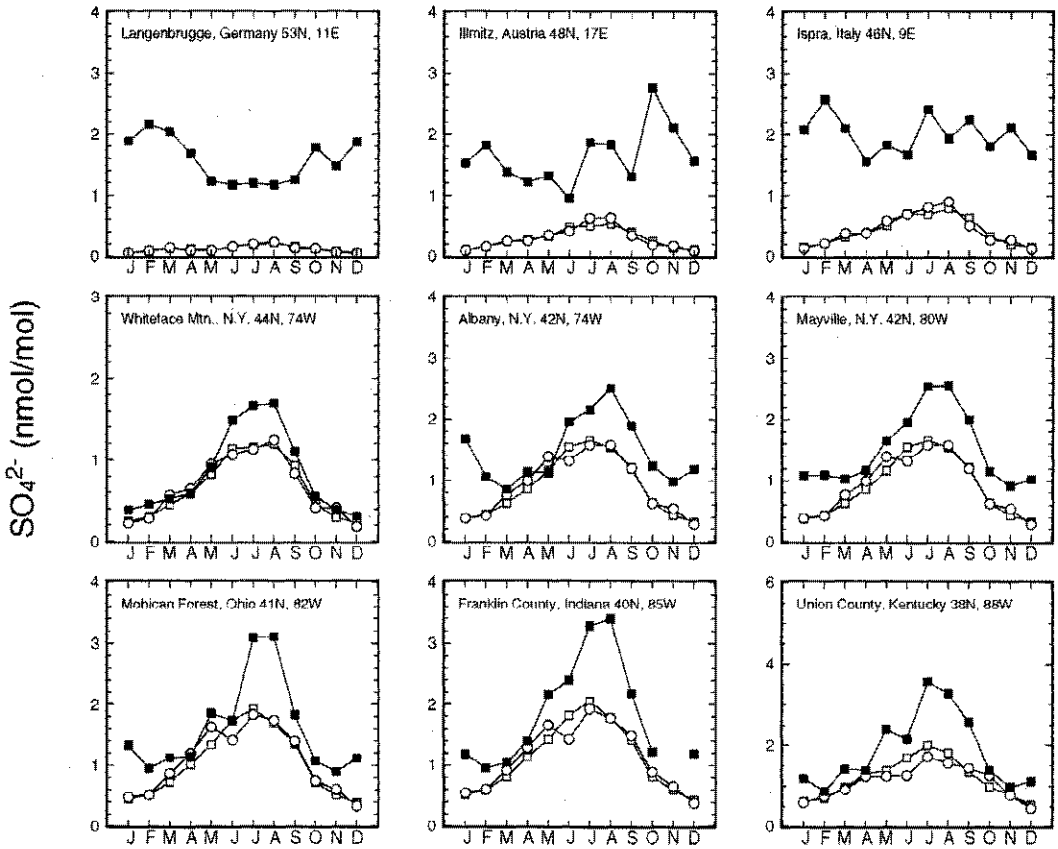

Figure 7a. Monthly averaged sulfate mixing ratio as a function of month at monitoring stations in Europe and the United States. Open squares are the model results for years 3–6 of the simulation, open circles are the model results for year 3 of the simulation, and solid squares are the observations. Measurements of non-sea-salt (nss)-SO_4^{2-} from EMEP sites in Europe from 1986 to 1992 [*Schaug et al.*, 1987], from Whiteface Mountain, New York, from 1975 to 1988, from Albany, New York, from July 1983 to February 1985, and from Mayville, New York, from 1981 to 1988 [*Husain and Dutkiewicz*, 1990], and from sites in Ohio, Indiana, and Kentucky from May 1980 to August 1981 [*Shaw and Paur*, 1983] are used for sites in the midlatitudes of Europe and the United States.

DMS chemistry, this comparison of modeled DMS and SO_2 to observed values suggests that there may be a sink of DMS that does not form SO_2.

Similar to *Chin et al.* [1996], we have compared our model results of SO_4^{2-} to observations from monitoring stations in Europe and the United States, in the Arctic and Subarctic, and in oceanic and Antarctic regions. In the United States, monthly mean SO_4^{2-} mixing ratios agree well with observations but are substantially less than observations at locations in Europe especially in winter (Figure 7a). Although modeled SO_2 agrees fairly well with observations at these stations (Figure 6), the underprediction of SO_4^{2-} in Europe could be due to underestimating the conversion of SO_2 to SO_4^{2-}, because a 1–2 nmol mol^{-1} decrease in SO_2 would still result in fairly good agreement between modeled and observed SO_2 and would increase modeled SO_4^{2-} mixing ratios to values that were observed. However, the sinks of SO_4^{2-} cannot be excluded as a possible explanation for underpredicting SO_4^{2-} in industrial Europe. These sinks could be either wet deposition or transport out of the boundary layer. The wet deposition of total sulfur, which mostly is SO_4^{2-} in our model [*Rasch et al.*, this issue], could explain some of the discrepancy for Langenbrugge in winter and summer and Illmitz and Ispra in winter because the modeled wet deposition for these two locations overestimates the observed wet deposition by factors of 1.3-2.6. However, this certainly is not enough to account for the factor 5 difference in surface mixing ratio; thus transport out of the bottom model level must also account for the discrepancy between modeled and observed SO_4^{2-} at the European sites.

Measurements of nss-SO_4^{2-} are used for comparison to modeled SO_4^{2-} at high latitude sites (Figure 7b). In Norway the model appears to exhibit a similar seasonal trend as the observations but underestimates the magnitude of the mixing ratios. Furthermore, there appears to be no correlation of the underestimation of modeled SO_4^{2-} with the comparable estimation of modeled SO_2 (Figure 6) for these Norwegian stations. Al-

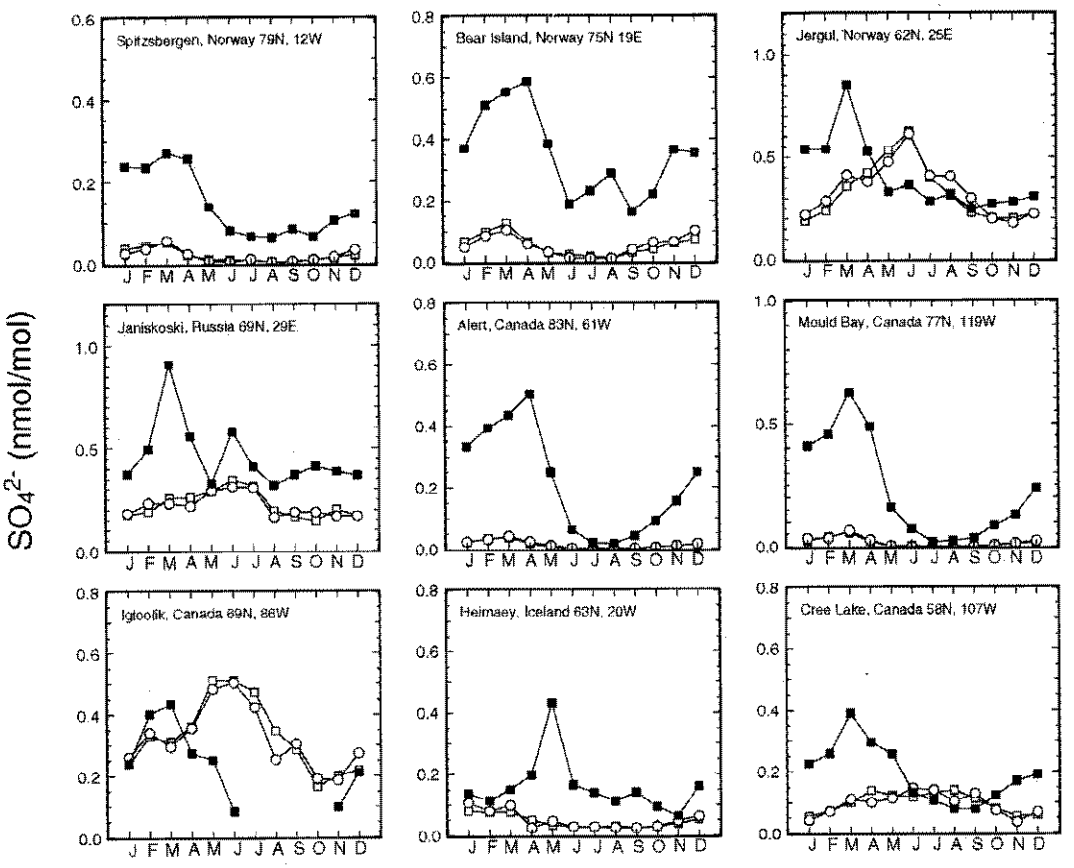

Figure 7b. Monthly averaged sulfate mixing ratio as a function of month at Arctic and Subarctic monitoring stations. Open squares are the model results for years 3–6 of the simulation, open circles are the model results for year 3 of the simulation, and solid squares are the observations. Measurements of nss-SO_4^{2-} are obtained from EMEP sites in Norway and Russia from 1986 to 1992 [*Schaug et al.*, 1987], from Bear Island, Norway, from 1978 to 1981 [*Heintzenberg and Larssen*, 1983], from Alert, Canada, from 1980 to 1990 [*Li and Barrie*, 1993], from Mould Bay and Igloolik, Canada, from 1979 to 1980 [*Barrie et al.*, 1989], from Heimaey, Iceland, from 1987 to 1993 [*Prospero et al.*, 1995, *Chin et al.*, 1996], and from Cree Lake, Canada, from 1982 to 1988 [*Barrie and Bottenheim*, 1990].

though modeled SO_2 mixing ratios are greater than observed at Jergul, Norway, the modeled SO_4^{2-} mixing ratios are either comparable or underestimate observed SO_4^{2-} mixing ratios. This would indicate that for these Norwegian sites the conversion of SO_2 to SO_4^{2-} is possibly underestimated, that wet deposition of SO_4^{2-} is too great, or that transport out of the boundary layer is too large in the description of the model. In summer, modeled sulfur wet deposition at Jergul, Norway, and Janiskoski, Russia, agree well with observed sulfur wet deposition (and the modeled and observed summer SO_4^{2-} mixing ratio agree fairly well). In winter the modeled sulfur wet deposition is much greater than observed (2.4 times greater at Jergul; 8 times greater at Janiskoski). This overestimation could account for the underestimation of surface SO_4^{2-} mixing ratios by the model in the Subarctic. In Canada the high concentrations of SO_4^{2-} in springtime are not evident from the model simulation. Without measurements of SO_2 or wet deposition of sulfur it is difficult to assess why modeled SO_4^{2-} is much less than observed in springtime. *Dastoor and Pudykiewicz* [1996] compared their modeled SO_4^{2-} to observations in Canada. Their model, which was driven by observed meteorological variables, captured the springtime maximum of SO_4^{2-} at Alert. Modeled SO_2 from *Dastoor and Pudykiewicz* [1996] also shows a large springtime maximum at Alert. Our modeled SO_2 at Alert also exhibits a maximum in spring, but the magnitude is much smaller than that found by *Dastoor and Pudykiewicz* [1996]. This indicates that the source of SO_4^{2-} in our model is not strong enough in northern Canada in springtime. Because there are no local anthropogenic sources of SO_2, the likely reason for underestimating springtime SO_4^{2-} at Alert is that the transport of SO_2 and SO_4^{2-} is not accurately represented in this region.

Measurements of nss-SO_4^{2-} are used for comparison to modeled SO_4^{2-} at oceanic and Antarctic sites. At monitoring stations located in the oceanic regions of the world, modeled aerosol sulfate concentrations are gen-

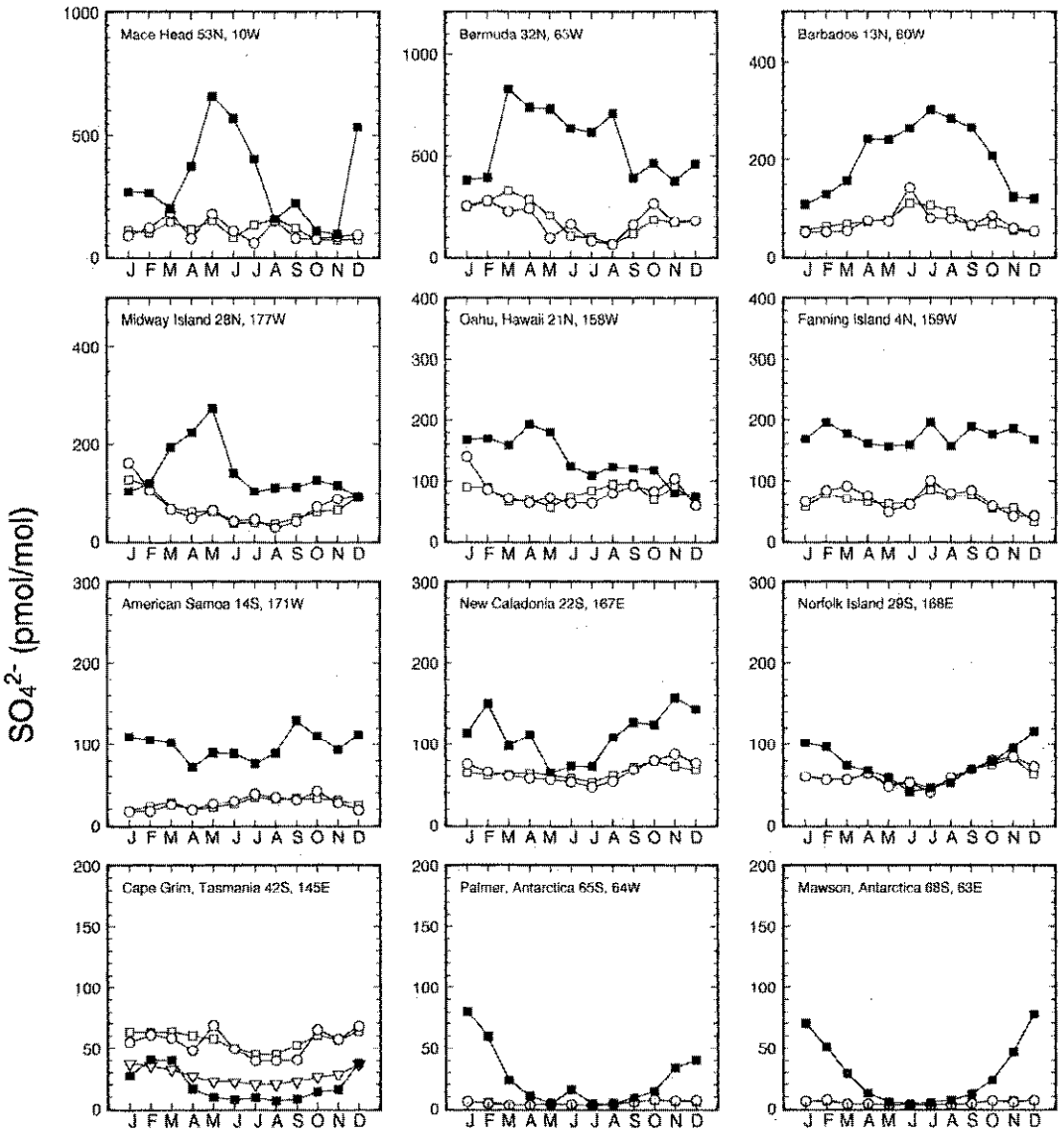

Figure 7c. Monthly averaged sulfate mixing ratio as a function of month at oceanic and Antarctic monitoring stations. Open squares are the model results for years 3–6 of the simulation, open circles are the model results for year 3 of the simulation, and solid squares are the observations. Open nablas for Cape Grim are years 3–6 modeled mixing ratios of biogenic sulfate. Measurements of SO_4^{2-} are obtained from Mace Head, Ireland, and Bermuda from 1988 to 1993 and Barbados from 1984 to 1993 [*Galloway et al.*, 1993, *Chin et al.*, 1996], from Midway Island and Oahu from 1981 to 1993 and Fanning Island from 1981 to 1987 [*Savoie et al.*, 1989, *Chin et al.*, 1996], from American Samoa from 1983 to 1985 [*Savoie et al.*, 1994], from New Caledonia from 1983 to 1985 and Norfolk Island from 1983 to 1990 [*Savoie et al.*, 1989, *Chin et al.*, 1996], from Cape Grim from 1976 to 1984 and 1988 to 1990 [*Ayers et al.*, 1986, 1991], from Palmer, Antarctica, from 1990 to 1991 and Mawson, Antarctica, from 1987 to 1991 [*Savoie et al.*, 1993].

erally less than observations, by as much as a factor of 6 (Figure 7c). Without measurements of DMS or SO_2 it is difficult to assess if the sources of SO_4^{2-} account for this underestimation. Model results indicate that the SO_4^{2-} found at these locations was produced primarily through in-cloud oxidation and that north of 20°N the SO_4^{2-} is primarily of anthropogenic origin. Because measurements at Cape Grim, Tasmania, were restricted to marine air masses [*Ayers et al.*, 1986], the SO_4^{2-} derived from biogenic sources is also plotted in Figure 7c. The agreement between measurements and modeled biogenic SO_4^{2-} at Cape Grim is greatly improved, although the modeled biogenic SO_4^{2-} does not exhibit so strong a seasonal cycle as the measurements. Most remote locations do not show strong seasonal trends in SO_4^{2-} concentrations; this behavior is captured by the model. At Bermuda and Barbados the model results indicate a small seasonal trend similar to the observa-

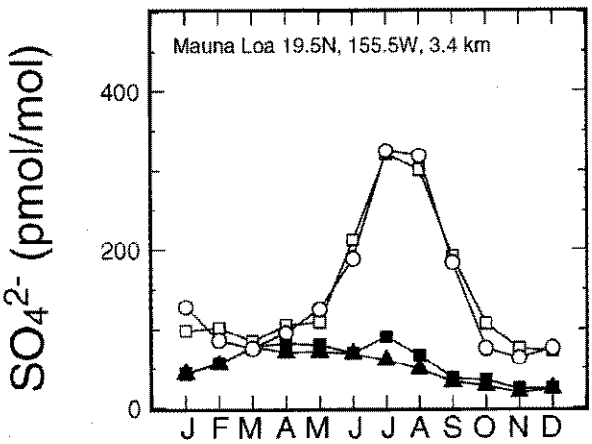

Figure 8. Monthly averaged sulfate mixing ratio in free tropospheric air at Mauna Loa Observatory. Open squares are the model results for years 3–6 of the simulation, and open circles are the model results for year 3 of the simulation. Solid triangles are averages of the daily measurements for which all four criteria (downslope winds, low condensation nuclei concentrations, low dew point, and low variability in CO_2) were met. Solid squares are the measurements for which three of the four criteria were met (B. Huebert, personal communication, 1998).

tions, but the trend from the model is much weaker than that seen in the observations. In Antarctica the model shows no seasonal trend, whereas the observations show an increase in sulfate during summer that is likely due to DMS chemistry.

Free tropospheric SO_4^{2-} mixing ratios obtained at Mauna Loa Observatory, averaged over 10 years of measurements (B. Huebert, personal communication, 1998) are generally lower than model results interpolated to the Mauna Loa location (Figure 8). This is especially true in June, July, and August for which the model shows that the sulfate originated from the North American continent, most likely the southwestern United States or northern Mexico (Plate 1). This plume from the North American continent travels west-southwest at 2-4 km in elevation, essentially the height of the Mauna Loa Observatory. The accuracy of the meteorological conditions in the model that produce the plume over the eastern Pacific from the North American continent is not certain. Therefore this SO_4^{2-} plume, evident in the model results, may not be real.

4.2. Balloon-Borne Measurements of Sulfate Aerosols

Hofmann [1993] assumed that the 20-year monthly averaged, balloon-borne measurements of aerosol backscatter were of aerosols composed of 75% H_2SO_4 (the rest being water). Because the atmospheric aerosol consists of different substances (e.g., sulfate, mineral dust, and carbon aerosols), the concentrations derived from the measured aerosol backscatter may overestimate the sulfate loading. These mass loadings of sulfuric acid aerosols are compared in Figure 9 to modeled sulfate mass loadings from years 3-6 of the integration. The observations and model results were separated into two layers, the lower layer from 2.5 to 5 km and an upper layer from 5 to 10 km. SO_4^{2-} loadings in the model exhibit seasonal patterns similar to the observations, but are somewhat lower than the observations throughout the year, partially because of other types of aerosols included in the measurements.

4.3. Aircraft Profiles of Prognosed Species

Vertical profiles of H_2O_2, DMS, SO_2, and SO_4^{2-} from the PEM-West A and B missions and the PEM-Tropics A mission were compared to results from years 3-6 of the model integration for the same regions (Figures 10-13). The measurements were grouped into regions so that three to four flights of data, which reflect a more representative measurement of the region and time of year, can be better compared to monthly mean model results from the entire region of observation (denoted in Figures 10-13). The grid points of the model that lie within each region were averaged to find a representative value of the observation region. The monthly average of each species was used to obtain a temporal representation of the measurement period.

Despite the simple manner by which H_2O_2 is predicted in the model, namely that H_2O_2 is generated from diurnally averaged HO_2 concentrations and that the model parameterization does not take into account cloud effects on H_2O_2 photolysis frequencies, the model results for the Pacific region are typically within 50% of observations (Figure 10). Although the model overestimates H_2O_2 concentrations in the western Pacific in February and March, the modeled values are within a

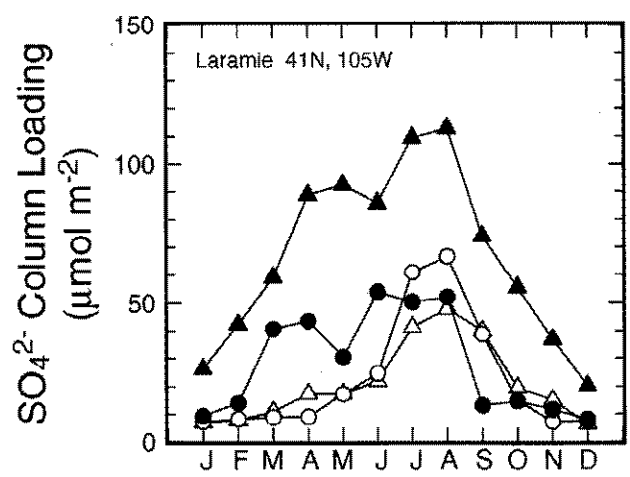

Figure 9. Monthly averaged sulfate column loading at Laramie, Wyoming. Open symbols are the model results, and closed symbols are the observations [*Hofmann*, 1993]. Triangles denote the column loading from 2.5 to 5 km above sea level, and circles denote the column loading from 5 to 10 km above sea level.

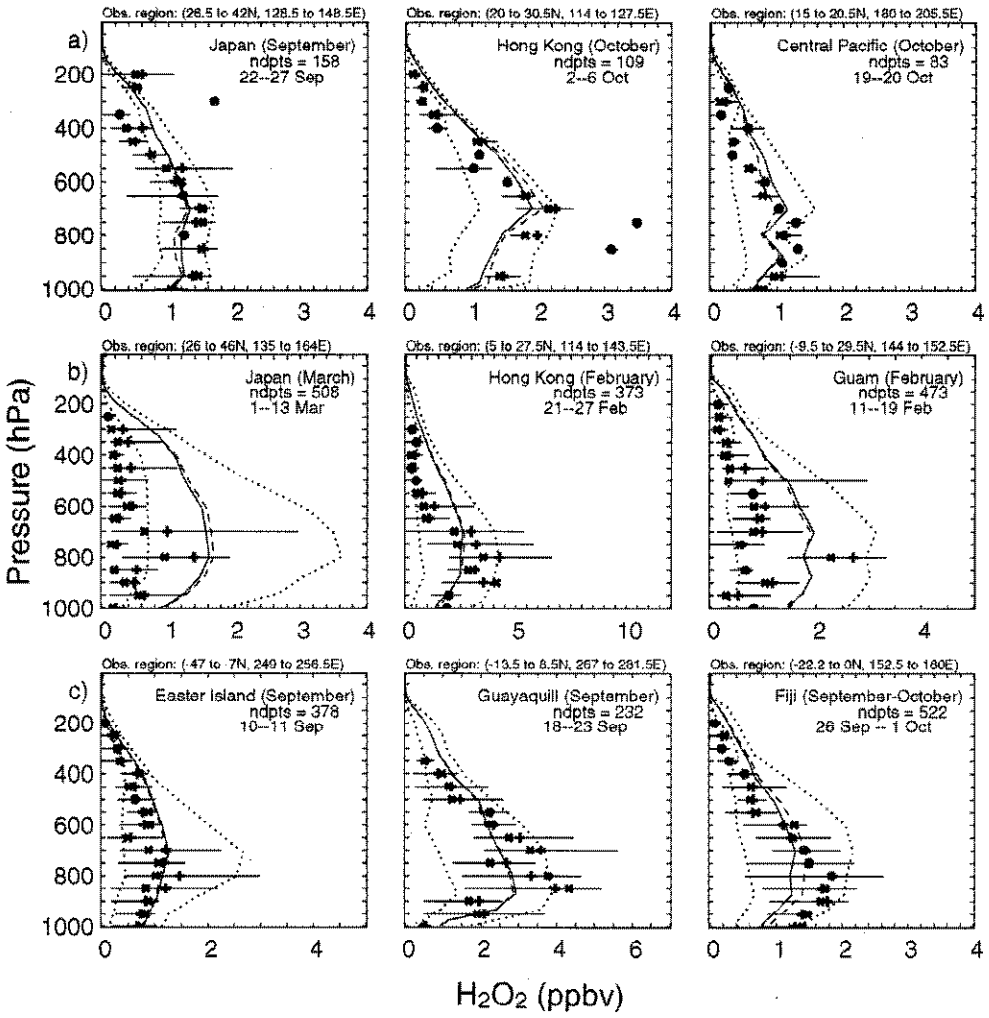

Figure 10. H_2O_2 mixing ratio versus height for the (a) Pacific Exploratory Mission (PEM)-West A, (b) PEM-West B, and (c) PEM-Tropics A research intensives. Monthly mean model results averaged over the observation region are indicated for years 3-6 (solid lines) and year 3 (dashed lines). Dotted lines are the minimum and maximum monthly mean mixing ratios from years 3-6 found in the observation region. Mean (pluses), median (crosses), 10th and 90th percentiles (bars) of the measurements from aircraft flights [*Heikes et al.*, 1996, *O'Sullivan et al.*, 1999] are indicated for every 50 hPa. Dates indicate the time period of observation and ndpts indicates the number of measurement points.

factor of 3 of the observations. Generally, the range of model values envelopes the means and medians of the observations in the Pacific Basin. Comparisons (not shown) of measured H_2O_2 concentrations in the northeast United States [*Tremmel et al.*, 1994], Switzerland [*Dommen et al.*, 1995], and Saxony, Germany [*Gnauk et al.*, 1997], to model results show good agreement in the boundary layer and free troposphere. It appears that H_2O_2 is predicted fairly well by the model in both remote and anthropogenically influenced regions.

In both observations and model results the vertical distribution of DMS in the Pacific region generally shows a high concentration near the surface, where DMS is emitted from the oceans, and low concentrations above the boundary layer (Figure 11). Because of the low solubility of DMS, it can be found in fairly high concentrations in the upper troposphere after convective activity. This is seen in the measurements near Japan during PEM-West A. The model results indicate convective activity in the PEM-West region during February and March, which is reflected to a small degree in the measurements. Overall, there is good agreement between measurements and model results for DMS in the Pacific Basin.

The agreement between model results and observations of the vertical distribution of SO_2 is variable (Figure 12). Results in the PEM-Tropics region are in good agreement with observations, but in the the PEM-West region, observations and the model results indicate a large amount of variability, and it is difficult to assess how well model results replicate observations. In the middle to upper troposphere, modeled SO_2 is in near

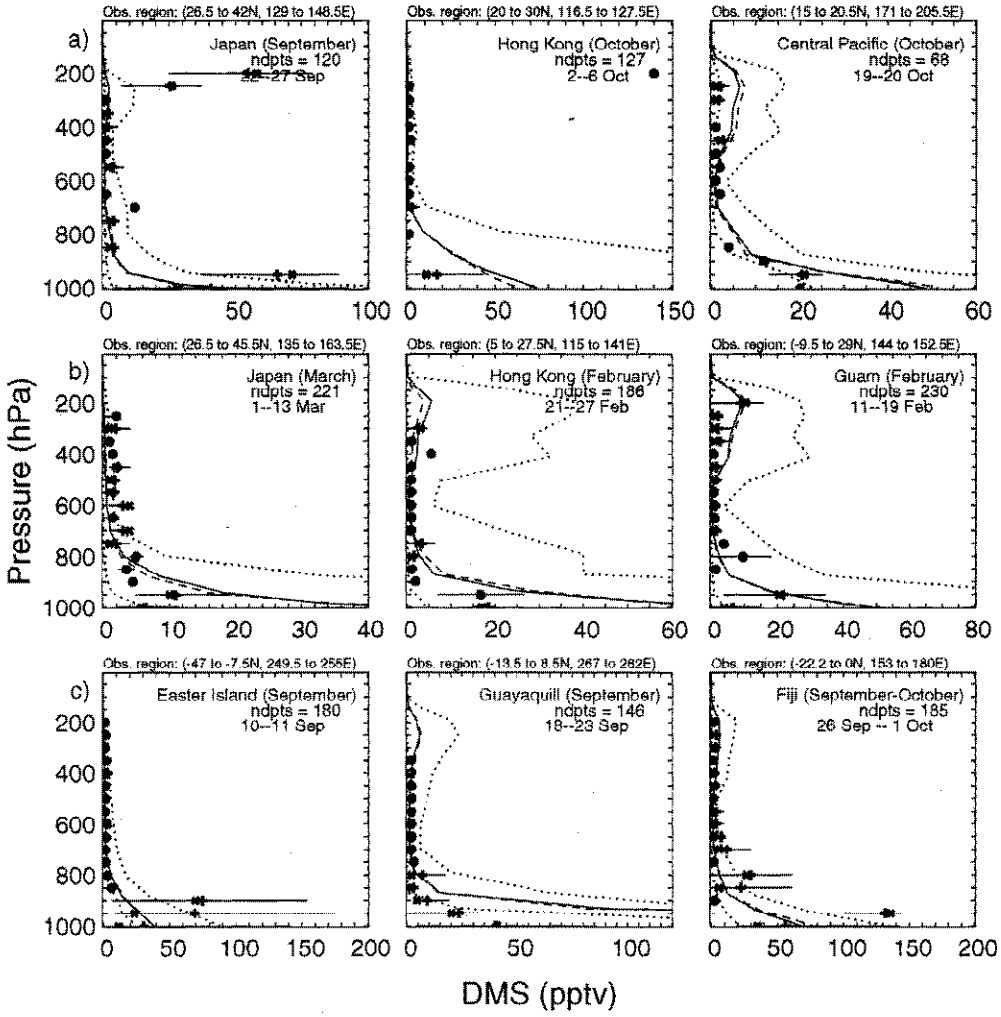

Figure 11. DMS mixing ratio versus height for the (a) PEM-West A, (b) PEM-West B, and (c) PEM-Tropics A research intensives. Monthly mean model results averaged over the observation region are indicated for years 3-6 (solid lines) and year 3 (dashed lines). Dotted lines are the minimum and maximum monthly mean mixing ratios from years 3-6 found in the observation region. Mean (pluses), median (crosses), 10th and 90th percentiles (bars) of the measurements from aircraft flights [*Thornton et al.*, 1996, 1997, 1999] are indicated for every 50 hPa. Dates indicate the time period of observation and ndpts indicates the number of measurement points.

agreement or underestimates observed SO_2. *Graf et al.* [1997] found that most of the SO_2 in the middle to upper troposphere was derived from volcanic emissions. Thus including volcanic emissions of SO_2 in this model would probably lead to modeled SO_2 values that are much larger than observed.

The variability of aerosol sulfate concentrations in both observations and model results is even more pronounced (Figure 13) than that of SO_2 concentrations. The model results show SO_4^{2-} concentrations in the Pacific region to be the same order of magnitude as the observations, but generally, the agreement between observations and model results of SO_4^{2-} is rather poor. Above the 400 hPa level the model tends to overestimate SO_4^{2-} mixing ratios, indicating that either the source of SO_4^{2-} to the upper troposphere (through transport processes) or the removal of SO_4^{2-} from the upper troposphere (through scavenging or sedimentation processes) may not be properly represented in our model. *Chin et al.* [1996], who performed a similar comparison for the PEM-West A region, found somewhat better agreement between their modeled and observed sulfate concentrations.

4.4. Satellite Measurements

Measurements from the SAGE satellite [*Kent et al.*, 1994] were constructed as the average of the background aerosol for years 1984–1991. The background aerosol was determined by fitting an exponential curve to the aerosol concentration following the El Chichon eruption and then subtracting this from the original time series of aerosol data [*Kent et al.*, 1995]. These background aerosol concentrations have been compared to modeled

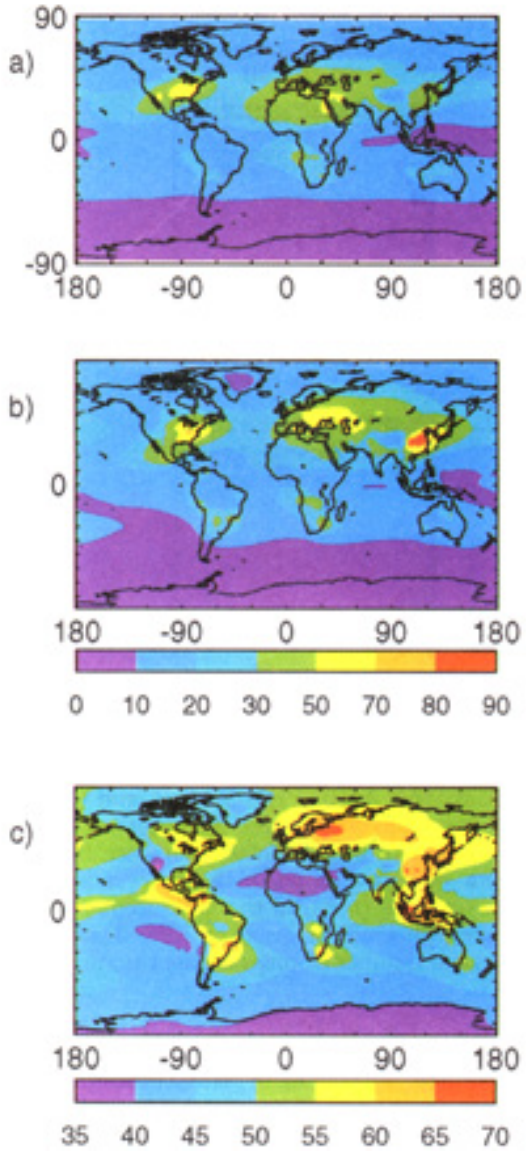

Plate 3. Annual-averaged column burden of sulfate produced (a) through gas-phase reaction (μmol m^{-2}) and (b) through aqueous-phase reaction. (c) Percent of the total sulfate column (sum of sulfate derived from primary emissions, gas-phase reaction, and aqueous-phase reaction) that is produced through aqueous-phase reaction.

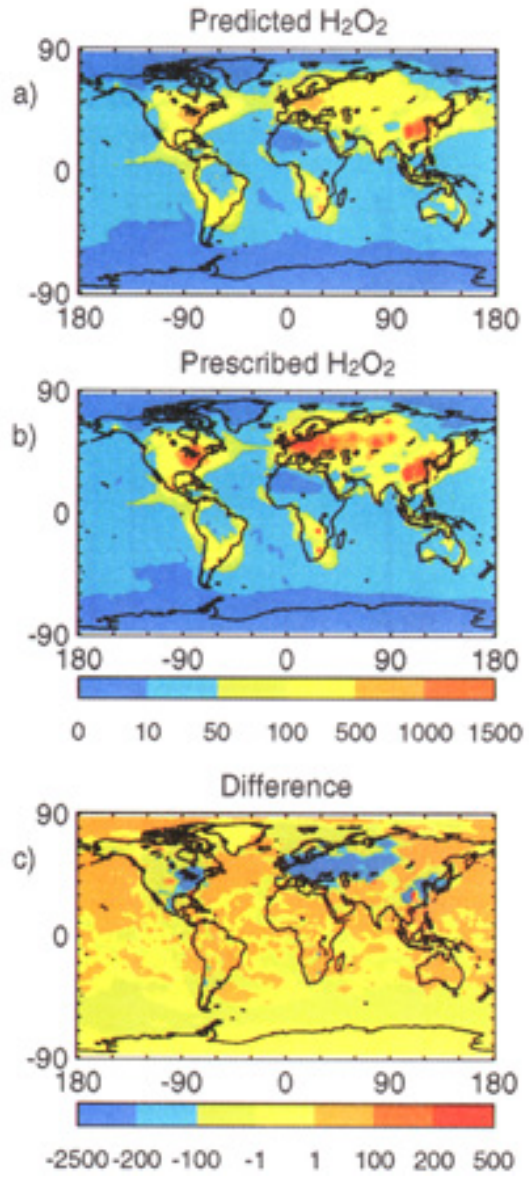

Plate 4. The annual-averaged vertical integral of the aqueous sink of H_2O_2 (pmol m^{-2} s^{-1}) for the simulation in which (a) H_2O_2 mixing ratios were allowed to be depleted and (b) H_2O_2 mixing ratios were prescribed by the Intermediate Model of Global Evolution of Species (IMAGES) model. (c) The results of the second simulation subtracted from those of the first.

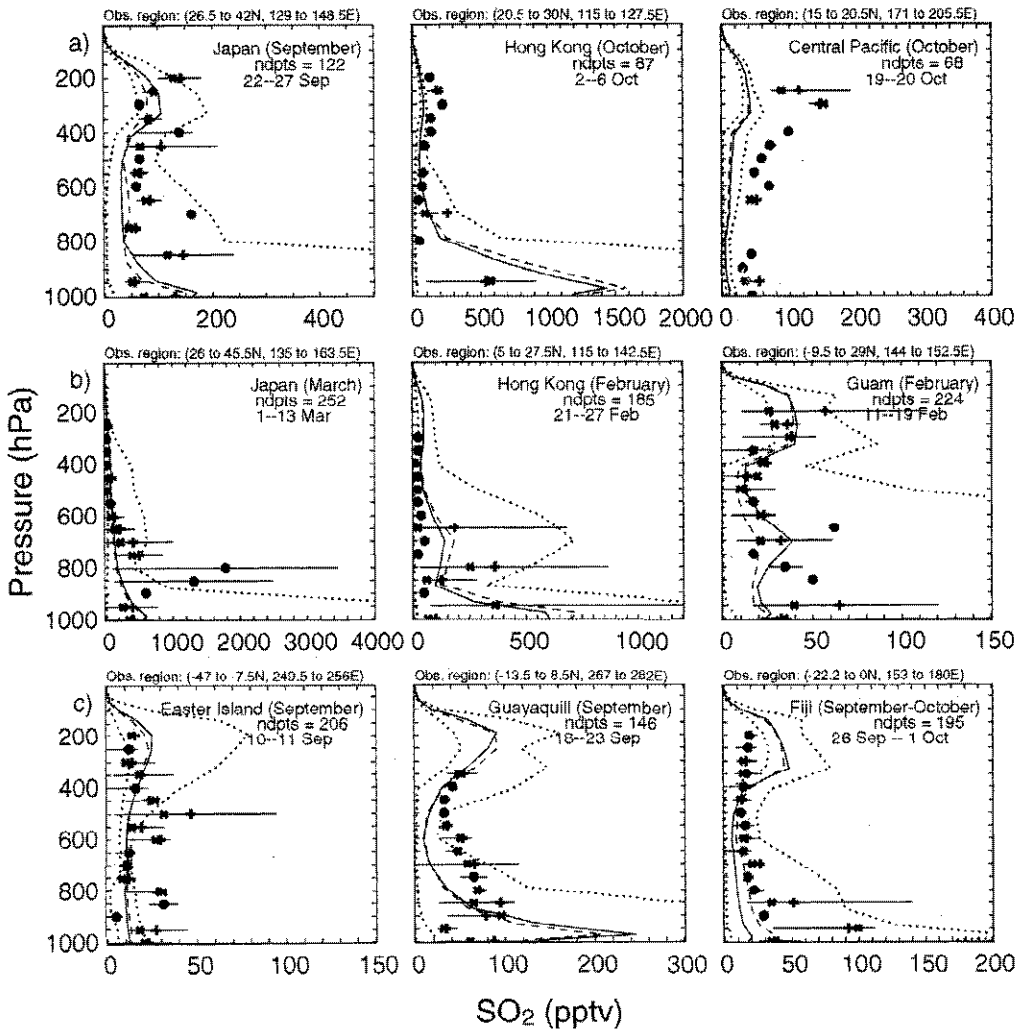

Figure 12. SO_2 mixing ratio versus height for the (a) PEM-West A, (b) PEM-West B, and (c) PEM-Tropics A research intensives. Monthly mean model results averaged over the observation region are indicated for years 3-6 (solid lines) and year 3 (dashed lines). Dotted lines are the minimum and maximum monthly mean mixing ratios from years 3-6 found in the observation region. Mean (pluses), median (crosses), 10th and 90th percentiles (bars) of the measurements from aircraft flights [*Thornton et al.*, 1996, 1997, 1999] are indicated for every 50 hPa. Dates indicate the time period of observation and ndpts indicates the number of measurement points.

sulfate aerosols from years 3-6 of the integration. Figure 14 illustrates a latitude versus height cross section of the annual average aerosol background concentration in the upper troposphere (7.5–15 km). SAGE measures total aerosol and thus may overestimate sulfate loadings in the upper troposphere. The SAGE measurements show in the tropics small concentrations of aerosol, which increase in concentration progressively toward the poles. *Kent et al.* [1995] found a springtime maximum at latitudes north of 20°N. They attribute this maximum between 20° and 40°N to dust and biomass burning aerosols. North of 40°N, they attribute the high concentrations to anthropogenic sources. However, this region exhibits downward transport of volcanic aerosol also; thus a small fraction of aerosols from the stratosphere likely resides in the midlatitude to poleward upper troposphere. Model results are less than the aerosol concentrations observed by SAGE; however, stratospheric sources (carbonyl sulfide and volcanic eruptions) of SO_4^{2-}, dust, or aerosols from biomass burning are not included in the model.

4.5. Summary of Comparisons

Overall, the model results for H_2O_2 showed good agreement with observations. DMS values predicted by the model were greater than those observed at monitoring stations located in high emissions areas, but good agreement was found with results from three aircraft missions in the Pacific Basin. The agreement between observations and model results for SO_2 and SO_4^{2-} were good at some locations but rather poor at other locations. Reasons for discrepancies could be omission

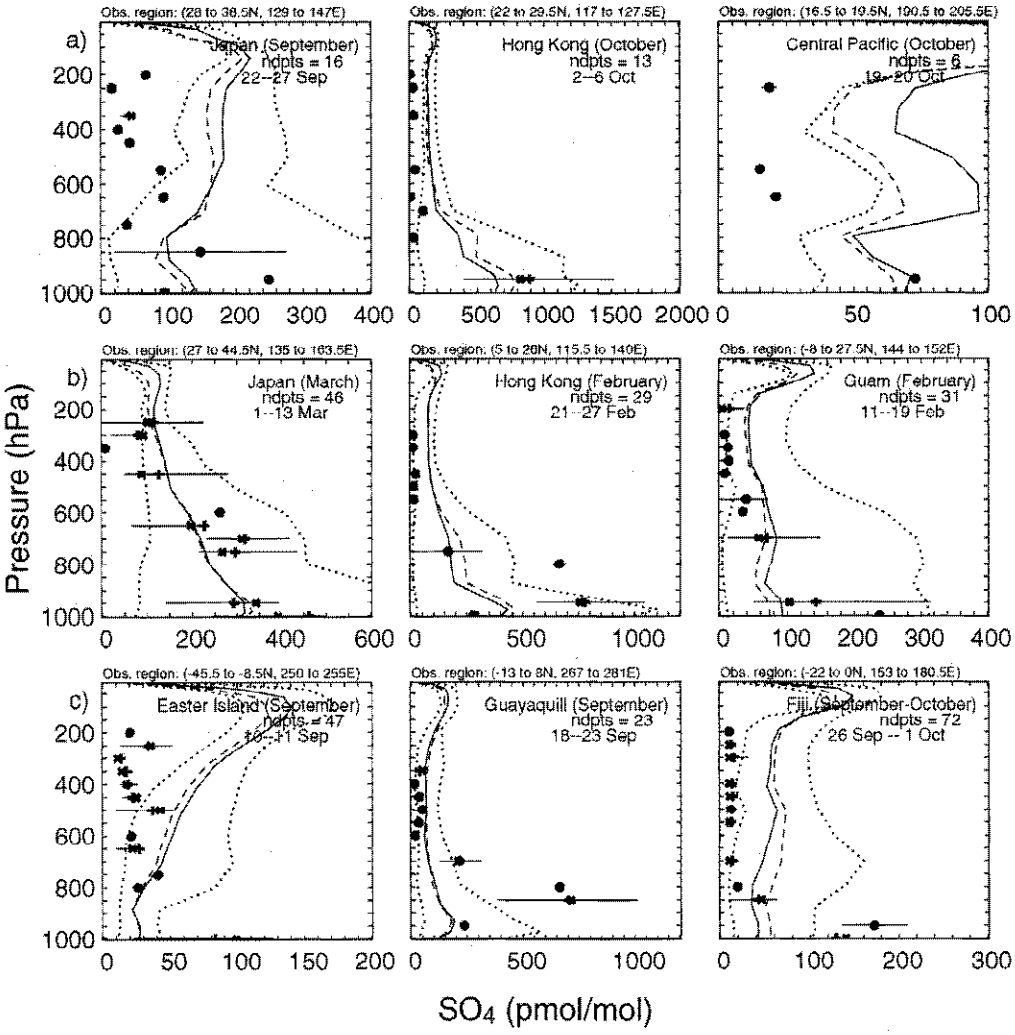

Figure 13. Sulfate mixing ratio versus height for the (a) PEM-West A, PEM-West B, and (c) PEM-Tropics A research intensives. Monthly mean model results averaged over the observation region are indicated for years 3-6 (solid lines) and year 3 (dashed lines). Dotted lines are the minimum and maximum monthly mean mixing ratios from years 3-6 found in the observation region. Mean (pluses), median (crosses), 10th and 90th percentiles (bars) of the measurements from aircraft flights [*Dibb et al.*, 1996, 1997, 1999] are indicated for every 50 hPa. Dates indicate the time period of observation and ndpts indicates the number of measurement points.

of other chemical reactions especially in industrial regions and the neglect of carbonyl sulfide and volcanic emissions, which contribute to the stratospheric and upper tropospheric sulfate loading [*Graf et al.*, 1997]. Driving the sulfur model with observed winds, such as with the Model of Atmospheric Transport and Chemistry (MATCH) [*Rasch et al.*, 1997], and comparing the model results to measurements for specific time periods would provide a more meaningful evaluation of the model.

5. Contribution of Sources to Sulfate

Following *Benkovitz et al.* [1994], we have tagged the SO_2 and SO_4^{2-} predicted in the model according to the chemical process that generated SO_2 or SO_4^{2-}. Results of the annual-averaged tagged sulfate from years 3-6 of the model integration are shown and discussed.

In the global budget of aerosol sulfate, 81% of the annual mean sulfate production rate, where anthropogenic emissions, gas-phase reactions, and aqueous-phase reactions contribute to the total sulfate production rate, was through aqueous-phase conversion of S(IV) to sulfate [*Rasch et al.*, this issue]. However, only 50% of the global annual mean aerosol sulfate burden was produced through the aqueous-phase reactions. This difference can be explained by the fact that a greater proportion of sulfate produced from aqueous-phase reaction than sulfate produced from gas-phase reaction is rapidly removed by wet deposition. As seen in the SO_4^{2-} column burdens (Plate 3), the location of sulfate produced through the aqueous and gas phases varies. The column

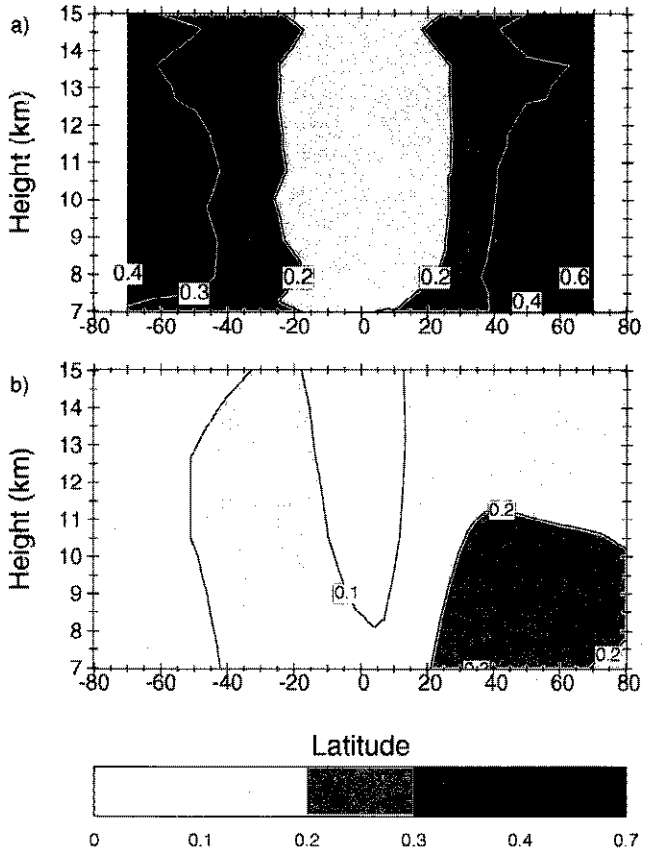

Figure 14. Annual-averaged zonal mean concentration versus height for (a) the background aerosol from Stratospheric Aerosol and Gas Experiment (SAGE) [*Kent et al.*, 1994] and (b) sulfate from the model.

burden of sulfate produced through the gas phase is greatest in the central United States and in the Mediterranean Sea region, whereas the column burden of sulfate produced through the aqueous phase is greatest over eastern Asia. The contribution of aqueous chemistry to the percent of the total sulfate (sum of the sulfate derived from primary emissions, gas-phase reactions, and aqueous-phase reactions) occurs primarily near regions of high sulfur emissions and frequent cloud occurrence (Indonesia and in the poleward midlatitudes). The zonal mean, annual-averaged sulfate (Figure 15) shows that sulfate produced through aqueous-phase oxidation resides mainly in and downwind of midlatitude stormtracks, whereas much of the sulfate produced from gas-phase oxidation resides mainly in drier locations (upper troposphere and northern subtropics).

6. Influence of Aqueous Chemistry

In the Northern Hemisphere industrial regions the primary contributor to the total sulfate is sulfate derived from aqueous-phase chemistry (Plate 3). Thus the formation of sulfate aerosols through aqueous chemistry is an important process to parameterize accurately in sulfur chemistry models. The liquid water content of the cloud water and rain, the ozone and hydrogen peroxide concentrations in the aqueous phase, and the pH of the drops are the important parameters in the aqueous-phase production of sulfate. The sensitivities of the sulfate burden to ozone concentrations and to liquid water contents are not examined as there is little influence of sulfur chemistry on ozone concentrations like there is on H_2O_2 concentrations, and therefore a strong sensitivity is not expected. Furthermore, it is difficult to alter the cloud water and rain mixing ratios in a climate model without altering other thermodynamic variables that could also affect the sulfur chemistry. H_2O_2 can be substantially affected by the sulfur chemistry. Acid deposition studies determined that for anthropogenically influenced regions the extent of SO_2 conversion to SO_4^{2-} can be limited by the available oxidants. Thus, in these regions during cloud events the H_2O_2 concentrations can be nearly completely depleted. To account for depleted H_2O_2 concentrations, we predicted H_2O_2 mixing ratios. To test the effect of using prescribed H_2O_2 values rather than predicted values, a sensitivity study was performed. In section 6.1, results of this sensitivity simulation are compared to the base simulation.

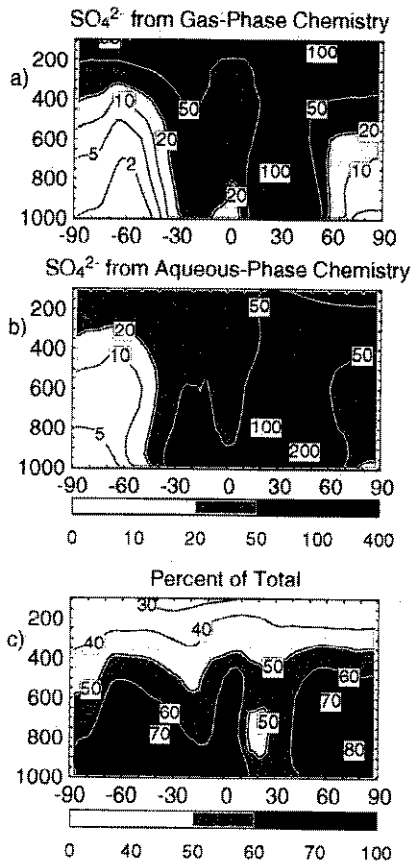

Figure 15. Zonal mean of the annually averaged sulfate mixing ratio (pmol mol^{-1}) produced (a) through gas-phase reaction and (b) through aqueous-phase reaction. (c) Percent of the total zonal mean sulfate burden that is produced through aqueous chemistry.

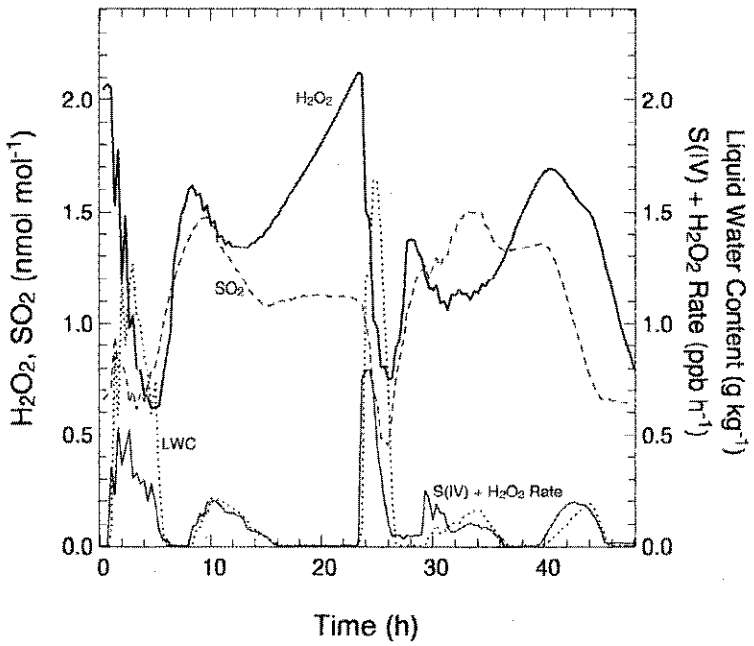

Figure 16. H_2O_2 (thick solid line) and SO_2 (dashed line) mixing ratios as a function of time at a single grid point (29.3°N, 121°E, 0.64 km altitude) in the Community Climate Model (CCM). These mixing ratios represent values for both clear-sky and cloudy regions of the grid cell and for the sum of the gas-phase and aqueous-phase concentrations. The dotted line is the liquid water content, indicating cloud events. The thin solid line is the S(IV) + H_2O_2 aqueous-phase reaction rate.

The rate of the S(IV) + O_3 aqueous reaction is pH dependent. At low pH the reaction rate is very slow, whereas at pH values above 5 the rate is fast. To account for the influence of a strong acid (SO_4^{2-}) produced in the oxidation of SO_2 on the rate of subsequent aqueous-phase reactions, the cloud water and rain pH is diagnosed at each time step of the aqueous chemistry. To test the sensitivity of this approach, a simulation was performed in which the pH was set to 4.5. Results of this simulation compared to the base run are discussed in section 6.2.

6.1. Sensitivity to H_2O_2

To determine how long it takes H_2O_2 concentrations to recover to precloud concentrations after a cloud event, we performed box model calculations for a 5-day integration under high- and low- SO_2 and NO_x conditions. The box model contains gas- and aqueous-phase reactions describing the diurnally varying chemistry of DMS, SO_x, NO_x, CH_4, and O_3. A cloud with a 0.2 g kg^{-1} cloud water mixing ratio was imposed from 0500 to 1000 LT on the first day of integration. The results showed that H_2O_2 concentrations decreased rapidly because of in-cloud conversion of S(IV) to S(VI) and recovered to pre-cloud concentrations 2 days after the cloud event. Certainly, clouds can exist for 5 hours or more, but a parcel of air does not remain in the cloud for that extensive period of time as is implied in a box model. Thus examination of grid points in the global model was done to determine the recovery time of H_2O_2 to photochemical equilibrium.

As an example of what is occurring in CCM3 with sulfur chemistry, a situation was found where clear sky initially occurred followed by clouds, with in-cloud oxidation of S(IV), and subsequent return to clear sky. The liquid water content, the concentrations of H_2O_2 and SO_2, and the S(IV) + H_2O_2 reaction rate through these events are shown in Figure 16. The liquid water content indicates the occurrence of clouds at this location. H_2O_2 and SO_2 were destroyed by aqueous reaction from hours 1 to 6 and then from hours 8 to 16. Clouds were absent at this grid point for 7 hours starting at hour 16. Nearly 70% of the H_2O_2 concentration was depleted during the first cloud event. Gas-phase production of H_2O_2 was nearly constant at 0.14 ppb h^{-1}, and gas-phase destruction of H_2O_2 was fairly constant at 0.05 ppb h^{-1}. During the 2 hours of clear sky, mostly advection and some chemical production of H_2O_2 occurred, bringing the concentration to 80% of its initial value. During the second cloud event, H_2O_2 again was depleted but only by ~12%. The H_2O_2 concentration returned to its initial value after the 7 hours of clear sky. This recovery can be attributed mainly to gas-phase production, but advection also plays a role in restoring the H_2O_2 mixing ratios. Again, after hour 23, H_2O_2 was destroyed by aqueous-phase reaction, and during this 25-hour period, H_2O_2 concentrations were appreciably below values in cloud-free air. From the

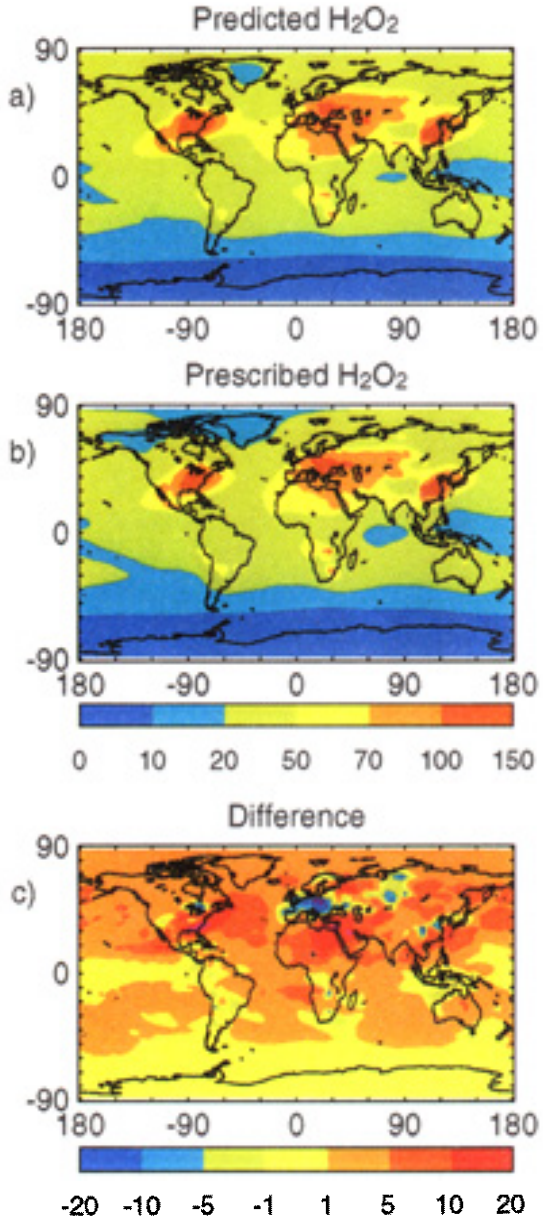

Plate 5. The annual-averaged sulfate column burden (μmol m^{-2}) for the simulation in which (a) H_2O_2 mixing ratios were allowed to be depleted and (b) H_2O_2 mixing ratios were prescribed by the IMAGES model. (c) The results of the second simulation subtracted from those of the first.

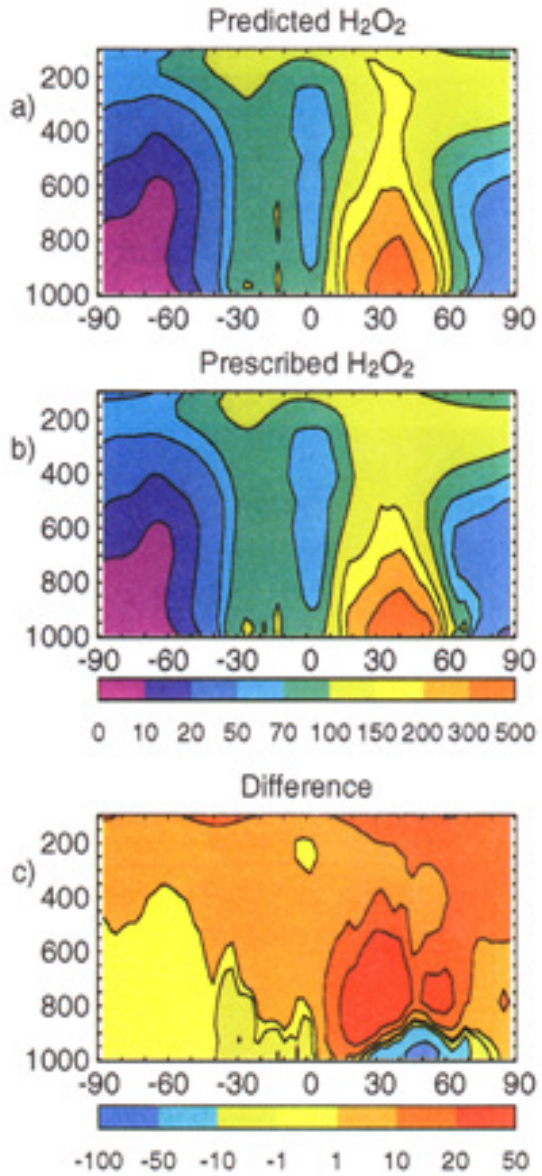

Plate 6. The zonally averaged annual mean sulfate mixing ratio (pmol mol^{-1}) for the simulation in which (a) H_2O_2 mixing ratios were predicted and (b) H_2O_2 mixing ratios were prescribed from the IMAGES model. (c) The results of the second simulation subtracted from those of the first.

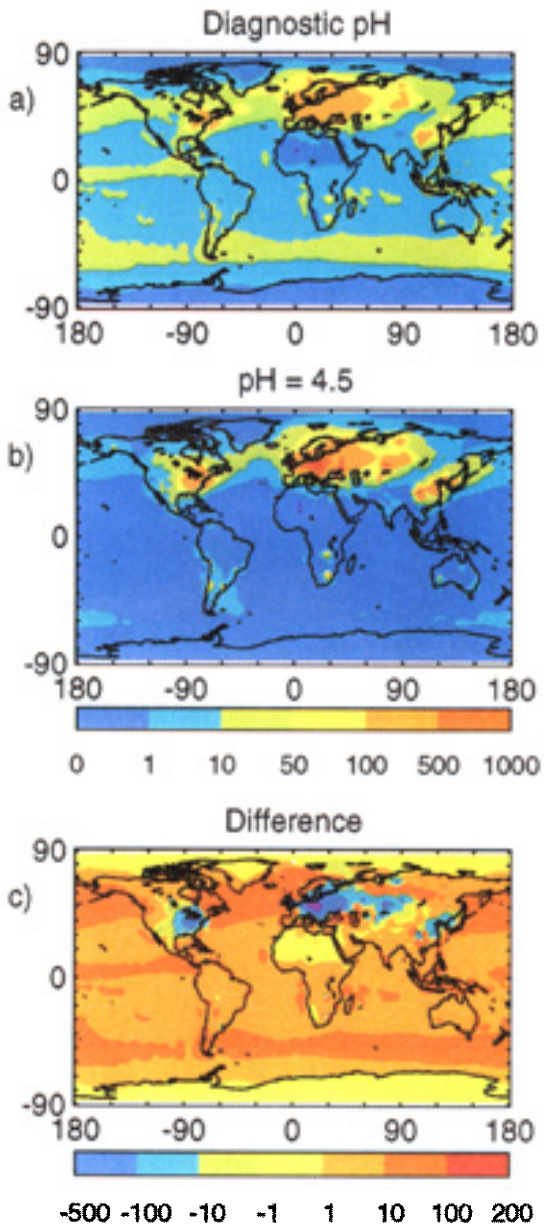

Plate 7. The annual-averaged column vertical integral of the rate of S(IV) + O_3 reaction (pmol m^{-2} s^{-1}) for the simulation in which (a) the pH was diagnosed and (b) the pH was set to 4.5. (c) The results of the second simulation subtracted from those of the first.

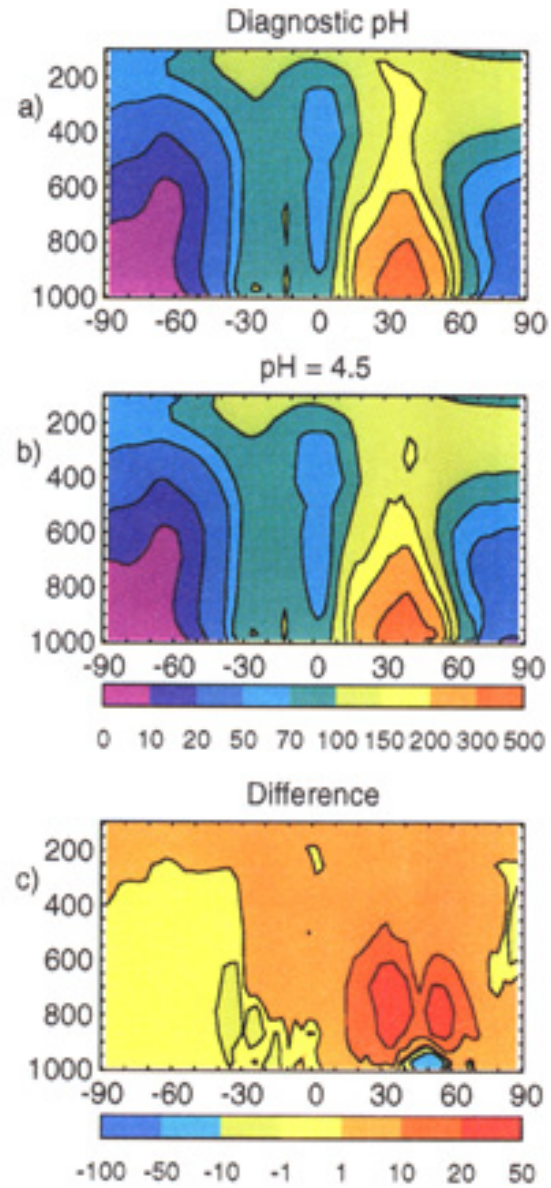

Plate 8. The zonally averaged annual mean sulfate mixing ratio (pmol mol^{-1}) for the simulation in which (a) the pH was diagnosed and (b) the pH was set to 4.5. (c) The results of the second simulation subtracted from those of the first.

Table 2. Global Sulfate Budget for Year 3 of the Simulation

	Base Run	Prescribed H_2O_2	pH = 4.5
Source, Tg S yr^{-1}	54.9	60.4	55.2
Primary Emissions, %	2.4	2.1	2.4
Gas-Phase Oxidation, %	16.8	12.3	15.4
In-cloud Oxidation, %	80.8	85.6	82.2
S(IV) + H_2O_2, %	65.1	79.5	68.8
S(IV) + O_3, %	15.7	6.1	13.4
Dry Deposition, %	6.7	6.5	6.5
Wet Deposition, %	93.3	93.5	93.5
Lifetime, days	3.8	3.2	3.6
Burden, Tg S	0.57	0.53	0.55
From gas-phase reaction, %	47	42	46
From aqueous-phase reaction, %	51	56	52

box model calculations and examining a grid point in the global model where clouds occurred, it is evident that after cloud events, H_2O_2 concentrations slowly increase to their photochemical clear-sky values. For the CCM, which uses a 20-min time step, it is therefore necessary to resolve H_2O_2 concentrations.

To examine the effect of using H_2O_2 concentrations that are depleted by chemical reaction versus those that were prescribed from monthly mean values that were determined from a gas-phase-only chemical transport model (IMAGES), a sensitivity simulation was performed. A comparison of the annual-averaged H_2O_2 concentration at levels below 2 km showed that H_2O_2 from IMAGES model output was less than that predicted by our model from 30°S to 40°N, but from 50°N and northward, H_2O_2 from IMAGES was greater than that predicted by our model. The difference in the northern latitudes can be particularly important for sulfate production in Europe and downwind of European sources. The column integral of the annual-averaged aqueous-phase S(IV) + H_2O_2 reaction rate for the simulation with the prescribed H_2O_2 concentrations, which are not depleted by aqueous reaction with SO_2, was greater in industrial regions of the world compared to the base simulation where H_2O_2 depletion was accounted for (Plate 4). If H_2O_2 is not allowed to be depleted, the in-cloud oxidation of S(IV) by H_2O_2 increases, as is found in the model results. As a further consequence, the rate of the S(IV) + O_3 reaction is substantially less in the simulation with prescribed H_2O_2 concentrations compared to the base simulation. The total aqueous-phase SO_4^{2-} production rate shows more aqueous-phase sulfate production in the simulation where H_2O_2 was prescribed than in the simulation where H_2O_2 was prognosed because the rate of S(IV) reaction with H_2O_2 is pH-independent and faster than the S(IV) + O_3 reaction for the pH range simulated in the model.

The sulfate column burden from the simulation where H_2O_2 is prescribed is less than the column burden from the base simulation (Plate 5). When H_2O_2 concentrations are prescribed, more in-cloud production occurs (Table 2), and therefore more sulfate is scavenged by precipitation. When H_2O_2 is allowed to be depleted, more gas-phase production of sulfate occurs (Table 2), allowing sulfate to be produced where it is less susceptible to scavenging. Consequently, the global sulfate burden has a larger contribution from SO_4^{2-} derived from gas-phase reaction for the simulation where H_2O_2 is allowed to be depleted (Table 2).

Decreases in aqueous-phase production of sulfate yield small decreases in the SO_4^{2-} burden derived from in-cloud production and relatively larger increases in the SO_4^{2-} burden derived from gas-phase reaction. Evidence for this is seen in Plate 6, in which more SO_4^{2-} is present at low altitudes, where in-cloud production dominates, for the simulation where H_2O_2 is prescribed. At higher altitudes, where gas-phase production dominates, more SO_4^{2-} is found from the simulation where H_2O_2 is allowed to be depleted. From Table 2 it is seen that prescribing the H_2O_2 mixing ratios reduces the global burden of sulfate by 7%, but Plates 5 and 6 show that prescribing the H_2O_2 mixing ratios has a larger effect in industrial regions. Therefore the distribution of sulfate is sensitive to the method of the H_2O_2 parameterization, but the global burden of sulfate is relatively insensitive to this parameterization.

Roelofs et al. [1998] performed a similar budget analysis for simulations with H_2O_2 calculated on-line and off-line of their sulfur chemistry and meteorology model.

They found for the region north of 30°N that in-cloud oxidation of SO_2 accounted for 78% of the SO_4^{2-} source when H_2O_2 was calculated on-line, for 87% of the SO_4^{2-} source when H_2O_2 was prescribed from an off-line model, and for 86% of the SO_4^{2-} source when H_2O_2 was prescribed from the on-line model. They also found that the SO_2 burden was largest for the simulation where H_2O_2 was calculated on-line and that the SO_4^{2-} burden in the region examined was essentially the same for all three simulations. This supports our conclusion that over a large region the method of H_2O_2 parameterization is not important to the amount of sulfate residing in the troposphere.

6.2. Sensitivity to pH

To determine the sensitivity of the sulfate burden to the pH of cloud water and rain used in the model calculations, we performed a second sensitivity simulation in which the pH was prescribed to a value of 4.5 instead of being evaluated from the dissolved SO_4^{2-} and SO_2 concentration. At pH = 4.5 the rate of the S(IV) + O_3 reaction is much greater in the industrial regions of the world compared to the base simulation (Plate 7). Note also that the S(IV) + O_3 reaction rate at pH = 4.5 is less in regions away from industrial regions than when pH is diagnosed. This changed reaction rate, in turn, affects the total aqueous-phase production rate in a similar manner. Because of the reason mentioned above, there is a small decrease in the sulfate column burden in regions downwind of eastern Europe in the simulation where pH = 4.5 compared to the base simulation. Plate 8 shows that increased in-cloud production of sulfate due to a constant pH increases the sulfate burden at low altitudes, but because less SO_2 is available for gas-phase reaction, there is a smaller burden of SO_4^{2-} in the middle and upper troposphere, leading to an overall smaller sulfate burden. There is a small change in the partitioning between SO_4^{2-} derived from gas-phase reaction and SO_4^{2-} derived from aqueous-phase reaction (Table 2). As can be seen in Table 2, the global sulfate burden is affected by <4% by prescribing the pH of the liquid hydrometeors. Thus, in a global sense, prescribing the pH of the cloud and rain is sufficient for determining the sulfate burden, but locally, especially in anthropogenically influenced regions such as the eastern United States and eastern Europe, the sulfate burden is sensitive to the pH of the cloud and rain drops.

7. Summary

Sulfur chemistry has been incorporated in the CCM3 in a manner that is internally consistent with other parameterizations in the model, most importantly with the parameterizations of the liquid water content and precipitation, which govern the aqueous-phase formation of sulfate and the removal of sulfate. The model predicts the concentrations of DMS, SO_2, SO_4^{2-}, and H_2O_2. Sources and sinks represented in the description of the sulfur cycle include emissions of DMS and anthropogenic sulfur, gas-phase oxidation of DMS and SO_2, gas-phase production and destruction of H_2O_2, aqueous-phase oxidation of S(IV) by H_2O_2 and O_3, dry deposition of H_2O_2, SO_2, and aerosol sulfate, and wet deposition of H_2O_2, SO_2, and aerosol sulfate. Modeled mixing ratios of H_2O_2 and DMS agree quite well with observations of these species that were measured in the Pacific Basin. Modeled mixing ratios of SO_2 agree reasonably with observations at various locations throughout the world but showed some overprediction in anthropogenically influenced regions. Modeled mixing ratios of aerosol sulfate agreed fairly well with observations in remote regions of the world but had distinct differences with observations in anthropogenically influenced regions and in the Arctic. In general, the simulation tended to underpredict sulfate concentrations at the surface and overpredict sulfate aloft. These discrepancies may be due to the chemistry being represented inaccurately or to the transport (especially in the polar regions).

Features of the base model simulation include SO_2 and SO_4^{2-} tagged by anthropogenic and biogenic sources and by SO_4^{2-} tagged by its production mechanism. Although the rate of the in-cloud oxidation accounts for 81% of the total sulfate production (sum of anthropogenic emissions, gas-phase reaction, and aqueous-phase reaction), sulfate that was produced by in-cloud oxidation of S(IV) accounts for only about half of the global sulfate burden. This situation is explained by rapid wet deposition removal of SO_4^{2-} that recently had been produced in the cloud water and rain. Sulfate generated by aqueous-phase reaction accounted for 50-90% of the total annual-averaged aerosol sulfate in the lower troposphere, whereas sulfate generated by gas-phase reaction was predominant in the upper troposphere.

Because in-cloud oxidation of S(IV) is the primary mechanism for producing aerosol sulfate in the lower troposphere, it is critical to represent this process accurately in models. The factors to which aqueous-phase sulfur chemistry can be sensitive are the cloud and rain liquid water contents, the O_3 and H_2O_2 concentrations, and the pH of cloud water and rain. Globally, the sulfate burden is not sensitive to the method used in representing H_2O_2 concentrations, but regionally, the sulfate burden is sensitive to the method. The global sulfate burden decreased by only 7% (up to 12% in the northern midlatitudes) when the S(IV) + H_2O_2 reaction rate increased by 34%. When in-cloud oxidation of S(IV) was increased, less SO_2 was available for gas-phase oxidation. This, in turn, decreased the burden of sulfate, particularly, in the middle and upper troposphere. The annual-averaged global sulfate burden was relatively insensitive to the pH of the cloud water and rain. The global sulfate burden decreased by 3.5% when

the aqueous-phase production rate of sulfate increased by 2.5% when the pH was fixed at 4.5. In regions influenced by industrial emissions the sulfate column burden decreased by up to 10% when the pH was fixed at 4.5. Both sensitivity simulations indicate that decreased in-cloud sulfate production tended to increase sulfate concentrations aloft and decrease sulfate concentrations at the surface. Surface sulfate predicted in the sensitivity simulations had similar concentrations as the base simulation and therefore also underpredicted observations.

Possible improvements in parameterization of the sulfur chemistry in the CCM3 include using an improved DMS emissions inventory, additional volcanic emissions of SO_2, additional SO_2 reactions, an improved treatment of DMS chemistry, and an improved representation of aerosol composition in which the NH_4^+ to SO_4^{2-} ratio would vary depending on the NH_3 concentration at each grid point location. The current version of the model predicts only the mass of SO_4^{2-} and does not include any representation of the size of the SO_4^{2-} or other physical properties that are critical to determining properties of the clouds or radiation. To calculate the radiative effect of the sulfate aerosol predicted by this model, *Kiehl et al.* [1999] used simple parameterizations to determine the size of the particles and cloud drops. Future applications of this model include allowing the sulfate aerosols to interact with the radiation and cloud microphysics for understanding the implications to the distribution of clouds, to the precipitation, and to the climate. Alternative anthropogenic sulfur emissions will be examined to determine the effect on the climate and cloud properties. The sulfur chemistry described will be incorporated in a model that is driven by observationally derived meteorological data [*Rasch et al.*, 1997] to compare model results with observations and to help analyze field program measurements.

Acknowledgments. We wish to thank P. Kasibhlata for providing the EMEFS and EMEP network data, M. Chin for providing the long-term monitoring stations data, the NASA GTE Web site for providing the aircraft data, B. Huebert for providing the measurements from the Mauna Loa Observatory, D. Hofmann for providing the balloon-borne aerosol measurements, and G. Kent for providing the SAGE satellite measurements. We thank Y. Zhang for helpful comments on the manuscript. NCAR is sponsored by the National Science Foundation. Work at BNL was supported by the Environmental Sciences Division of the U.S. Department of Energy and was performed under contract DE-AC02-98CH10886.

References

Albrecht, B. A., Aerosols, cloud microphysics, and fractional cloudiness, *Science*, *245*, 1227–1230, 1989.

Ayers, G. P., J. P. Ivey, and H. S. Goodman, Sulfate and methanesulfonate in the maritime aerosol at Cape Grim, Tasmania, *J. Atmos. Chem.*, *4*, 173–185, 1986.

Ayers, G. P., J. P. Ivey, and R. W. Gillett, Coherence between seasonal cycles of dimethyl sulfide, methanesulphonate and sulphate in marine air, *Nature*, *349*, 404–406, 1991.

Balkanski, Y. J., D. J. Jacob, G. M. Gardner, W. C. Graustein, and K. K. Turekian, Transport and residence times of tropospheric aerosols inferred from a global three-dimensional simulation of ^{210}Pb, *J. Geophys. Res.*, *98*, 20,573–20,586, 1993.

Barrie, L. A., and J. W. Bottenheim, Sulphur and nitrogen pollution in the Arctic atmosphere, in *Pollution of the Arctic Atmosphere*, edited by W. T. Sturges, pp. 155–181, Elsevier, New York, 1990.

Barrie, L. A., M. P. Olson, and K. K. Oikawa, The flux of anthropogenic sulphur into the Arctic from mid-latitudes in 1979/80, *Atmos. Environ.*, *23*, 2505–2512, 1989.

Barth, M. C., D. A. Hegg, and P. V. Hobbs, Numerical modeling of cloud and precipitation chemistry associated with two rainbands and some comparisons with observations, *J. Geophys. Res.*, *97*, 5825–5845, 1992.

Bates, T. S., B. K. Lamb, A. Guenther, J. Dignon, and R. E. Stoiber, Sulfur emissions from natural sources, *J. Atmos. Chem.*, *14*, 315–337, 1992.

Benkovitz, C. M., C. M. Berkowitz, R. C. Easter, S. Nemesure, R. Wagener, and S. E. Schwartz, Sulfate over the North Atlantic and adjacent continental regions: Evaluation for October and November 1986 using a three-dimensional model driven by observation-derived meteorology, *J. Geophys. Res.*, *99*, 20,725–20,756, 1994.

Benkovitz, C. M., M. T. Scholtz, J. Pacyna, L. Tarrason, J. Dignon, E. C. Voldner, P. A. Spiro, J. A. Logan, and T. E. Graedel, Global gridded inventories of anthropogenic emissions of sulfur and nitrogen, *J. Geophys. Res.*, *101*, 29,239–29,254, 1996.

Boers, R., G. P. Ayers, and J. L. Gras, Coherence between seasonal variation in satellite-derived cloud optical depth and boundary layer CCN concentrations at a mid-latitude Southern Hemisphere station, *Tellus, Ser. B*, *46*, 123–131, 1994.

Carmichael, G. R., L. K. Peters, and T. Kitada, A second generation model for regional-scale transport/chemistry/deposition, *Atmos. Environ.*, *20*, 173–188, 1986.

Chang, J. S., R. A. Brost, I. S. A. Isaksen, S. Madronich, P. Middleton, W. R. Stockwell, and C. J. Walcek, A three-dimensional Eulerian acid deposition model: Physical concepts and formulation, *J. Geophys. Res.*, *92*, 14,681–14,700, 1987.

Charlson, R. J., J. E. Lovelock, M. O. Andreae, and S. G. Warren, Oceanic phytoplankton, atmospheric sulphur, cloud albedo and climate, *Nature*, *326*, 655–661, 1987.

Charlson, R. J., J. Langner, H. Rodhe, C. B. Leovy, and S. G. Warren, Perturbation of the Northern Hemisphere radiative balance by backscattering from anthropogenic sulfate aerosols, *Tellus, Ser. A*, *43*, 152–163, 1991.

Chaumerliac, N., E. Richard, J.-P. Pinty, and E. C. Nickerson, Sulfur scavenging in a mesoscale model with quasi-spectral microphysics: Two-dimensional results for continental and maritime clouds, *J. Geophys. Res.*, *92*, 3114–3126, 1987.

Chin, M., D. J. Jacob, G. M. Gardner, M. S. Foreman-Fowler, P. A. Spiro, and D. L. Savoie, A global three-dimensional model of tropospheric sulfate, *J. Geophys. Res.*, *101*, 18,667–18,690, 1996.

Coakley, J. A., R. L. Bernstein, and P. A. Durkee, Effect of ship stack effluents on the radiative properties of marine stratocumulus: Implications for man's impact on climate, in *Aerosols and Climate*, edited by P. V. Hobbs and M. P. McCormick, pp. 253–260, A. Deepak, Hampton, Va., 1988.

Cowling, E. B., Acid precipitation in historical perspective, *Environ. Sci. Technol.*, *16*, 110A–123A, 1982.

Dana, T. M., and J. M. Hales, Statistical aspects of the washout of polydisperse aerosols, *Atmos. Environ.*, *10*, 45–50, 1976.

Dastoor, A. P., and J. Pudykiewicz, A numerical global meteorological sulfur transport model and its application to Arctic air pollution, *Atmos. Environ.*, *30*, 1501–1522, 1996.

Demore, W. B., S. P. Sander, C. J. Howard, A. R. Ravishankara, D. M. Golden, C. E. Kolb, R. F. Hampson, M. J. Kurylo, and M. J. Molina, Chemical kinetics and photochemical data for use in stratospheric modeling: Evaluation number 12, *JPL Publ.*, *97-4*, 266pp., 1997.

Dibb, J. E., R. W. Talbot, K. I. Klemm, G. L. Gregory, H. B. Singh, J. D. Bradshaw, and S. T. Sandholm, Asian influence over the western North Pacific during fall season: Inferences from lead 210, soluble ionic species, and ozone, *J. Geophys. Res.*, *101*, 1779–1792, 1996.

Dibb, J. E., R. W. Talbot, B. L. Lefer, E. M. Scheuer, G. L. Gregory, E. V. Browell, J. D. Bradshaw, S. T. Sandholm, and H. B. Singh, Distributions of beryllium-7, lead-210, and soluble aerosol-associated ionic species over the western Pacific: PEM-West B, February–March, 1994, *J. Geophys. Res.*, *102*, 28,287–28,302, 1997.

Dibb, J. E., R. W. Talbot, E. M. Scheuer, D. R. Blake, N. J. Blake, G. L. Gregory, G. W. Sachse, and D. C. Thornton, Aerosol chemical composition and distribution during the Pacific Exploratory Mission (PEM) Tropics, *J. Geophys. Res.*, *104*, 5785–5800, 1999.

Dommen, J., A. Neftel, A. Sigg, and D. J. Jacob, Ozone and hydrogen peroxide during summer smog episodes over the Swiss Plateau: Measurements and model simulations, *J. Geophys. Res.*, *100*, 8953–8966, 1995.

Feichter, J., E. Kjellström, H. Rodhe, F. Dentener, J. Lelieveld, and G.-J. Roelofs, Simulation of the tropospheric sulfur cycle in a global climate model, *Atmos. Environ.*, *30*, 1693–1707, 1996.

Galloway, J. N., D. L. Savoie, W. C. Keene, and J. M. Prospero, The temporal and spatial variability of scavenging ratios for nss-sulfate, nitrate, methanesulfonate and sodium in the atmosphere over the North Atlantic Ocean, *Atmos. Environ.*, *27A*, 235–250, 1993.

Gnauk, T., W. Rolle, and G. Spindler, Diurnal variations of atmospheric hydrogen peroxide concentrations in Saxony (Germany), *J. Atmos. Chem.*, *27*, 79–103, 1997.

Graf, H.-F., J. Feichter, and B. Langmann, Volcanic sulfur emissions: Estimates of source strength and its contribution to the global sulfate distribution, *J. Geophys. Res.*, *102*, 10,727–10,738, 1997.

Hack, J. J., Parameterization of moist convection in the NCAR Community Climate Model, CCM2, *J. Geophys. Res.*, *99*, 5551–5568, 1994.

Hegg, D. A., S. A. Rutledge, P. V. Hobbs, M. C. Barth, and O. Hertzmann, The chemistry of a mesoscale rainband, *Q. J. R. Meteorol. Soc.*, *115*, 867–886, 1989.

Hegg, D. A., R. J. Ferek, P. V. Hobbs, and L. F. Radke, Dimethyl sulfide and cloud condensation nucleus correlations in the northeast Pacific Ocean, *J. Geophys. Res.*, *96*, 13,189–13,191, 1991a.

Hegg, D. A., L. F. Radke, and P. V. Hobbs, Measurements of Aitken nuclei and cloud condensation nuclei in the marine atmosphere and their relation to the DMS-cloud-climate hypothesis, *J. Geophys. Res.*, *96*, 18,727–18,733, 1991b.

Heikes, B. G., et al., Hydrogen peroxide and methylhydroperoxide distributions related to ozone and odd hydrogen over the North Pacific in the fall of 1991, *J. Geophys. Res.*, *101*, 1891–1906, 1996.

Heintzenberg, J., and S. Larssen, SO_2 and SO_4^{2-} in the Arctic: Interpretation of observations at three Norwegian Arctic-Subarctic stations, *Tellus, Ser. B*, *35*, 255–265, 1983.

Hesstvedt, E., O. Hov, and I. S. A. Isaksen, Quasi-steady-state approximation in air pollution modeling: Comparison of two numerical schemes of oxidant prediction, *Int. J. Chem. Kinet.*, *10*, 971–994, 1978.

Hoffmann, M. R., and J. G. Calvert, Chemical transportation modules for Eulerian acid deposition models, vol. II, The aqueous-phase chemistry, *Rep. EPA/600/3-85/017*, Environ. Prot. Agency, Research Triangle Park, N. C., 1985.

Hofmann, D. J., Twenty years of balloon-borne tropospheric aerosol measurements at Laramie, Wyoming, *J. Geophys. Res.*, *98*, 12,753–12,776, 1993.

Husain, L., and V. A. Dutkiewicz, A long-term (1975-1988) study of atmospheric SO_4^{2-}: Regional contributions and concentration trends, *Atmos. Environ.*, *24A*, 1175–1187, 1990.

Kasibhatla, P., W. L. Chameides, and J. S. John, A three-dimensional global model investigation of seasonal variations in the atmospheric burden of anthropogenic sulfate aerosols, *J. Geophys. Res.*, *102*, 3737–3760, 1997.

Keene, W. C., D. J. Jacob, and S.-M. Fan, Reactive chlorine: A potential sink for dimethylsulfide and hydrocarbons in the marine boundary layer, *Atmos. Environ.*, *30*, i–iii, 1996.

Kent, G. S., M. P. McCormick, and P.-H. Wang, Validation of Stratospheric Aerosol and Gas Experiments I and II satellite aerosol optical depth measurements using surface radiometer data, *J. Geophys. Res.*, *99*, 10,333–10,339, 1994.

Kent, G. S., P.-H. Wang, M. P. McCormick, and K. M. Skeens, Multiyear Stratospheric Aerosol and Gas Experiment II measurements of upper tropospheric aerosol characteristics, *J. Geophys. Res.*, *100*, 13,875–13,899, 1995.

Kiehl, J. T., J. J. Hack, G. B. Bonan, B. A. Boville, D. L. Williamson, and P. J. Rasch, The National Center for Atmospheric Research Community Climate Model: CCM3, *J. Clim.*, *11*, 1131–1150, 1998.

Kiehl, J. T., T. L. Schneider, P. J. Rasch, M. C. Barth, and J. Wong, Radiative forcing due to sulfate simulations with the National Center for Atmospheric Research Community Climate Model, Version 3, *J. Geophys. Res.*, in press, 1999.

Langner, J., and H. Rodhe, A global three-dimensional model of the tropospheric sulfur cycle, *J. Atmos. Chem.*, *13*, 225–263, 1991.

Li, S.-M., and L. A. Barrie, Biogenic sulfur aerosol in the Arctic troposphere, 1, Contributions to total sulfate, *J. Geophys. Res.*, *98*, 20,613–20,622, 1993.

Lind, J. A., and G. L. Kok, Henry's law determination for aqueous solutions of hydrogen peroxide, methyl hydroperoxide, and peroxyacetic acid, *J. Geophys. Res.*, *91*, 7889–7896, 1986.

Maahs, H. G., Sulfur dioxide/water equilibrium between 0° and 50°C: An examination of data at low concentrations, in *Heterogeneous Atmospheric Chemistry, Geophys. Monogr. Ser.*, edited by D. R. Schryer, vol. 26, 273, AGU, Washington, D. C., 1982.

Marshall, J. S., and W. M. Palmer, The distribution of raindrops with size, *J. Meteorol.*, *5*, 165–166, 1948.

McNaughton, D. J., and R. J. Vet, Eulerian model evaluation field study (EMEFS): A summary of surface network measurements and data quality, *Atmos. Environ.*, *30*, 227–238, 1996.

Müller, J.-F., and G. P. Brasseur, IMAGES: A three-dimensional chemical transport model of the global troposphere, *J. Geophys. Res.*, *100*, 16,455–16,490, 1995.

National Bureau of Standards, Selected values of chemical thermodynamic properties, 1, *Tech. Note 270-1*, Gaithersburg, Md., 1965.

Nguyen, B. C., N. Mihalopoulos, J. P. Putaud, A. Gaudry, L. Gallet, W. C. Keene, and J. N. Galloway, Covariations in oceanic dimethyl sulfide, its oxidation products and rain acidity at Amsterdam Island in the southern Indian Ocean, *J. Atmos. Chem.*, *15*, 39–53, 1992.

O'Sullivan, D. W., B. G. Heikes, M. Lee, W. Chang, G. E. Gregory, D. R. Blake, and G. Sachse, The distribution of hydrogen peroxide and methylhydroperoxide over the Pacific and South Atlantic Oceans, *J. Geophys. Res.*, *104*, 5635–5646, 1999.

Pham, M., J.-F. Müller, G. Brasseur, C. Granier, and G. Megie, A three-dimensional study of the tropospheric sulfur cycle, *J. Geophys. Res.*, *100*, 26,061–26,092, 1995.

Prospero, J. M., D. L. Savoie, R. Arimoto, H. Olafsson, and H. Hjartarson, Sources of aerosol nitrate and non-sea-salt sulfate in the Iceland region, *Sci. Total Environ.*, *160/161*, 181–191, 1995.

Radke, L. F., In situ measurements of ship tracks, in *Annalen der Meteorologie*, pp. 121–123, Offenbach, Germany, 1988.

Rasch, P. J., and J. E. Kristjánsson, A comparison of the CCM3 model climate using diagnosed and predicted condensate parameterizations, *J. Clim.*, *11*, 1587–1614, 1998.

Rasch, P. J., N. M. Mahowald, and B. E. Eaton, Representations of transport, convection, and the hydrologic cycle in chemical transport models: Implications for the modeling of short-lived and soluble species, *J. Geophys. Res.*, *102*, 28,127–28,138, 1997.

Rasch, P. J., M. C. Barth, and J. T. Kiehl, A description of the global sulfur cycle and its controlling processes in the NCAR CCM3, *J. Geophys. Res.*, this issue.

Roelofs, G.-J., J. Lelieveld, and L. Ganzeveld, Simulation of global sulfate distribution and the influence on effective cloud drop radii with a coupled photochemistry-sulfur cycle model, *Tellus, Ser. B*, *50*, 224–242, 1998.

Savoie, D. L., J. M. Prospero, and E. S. Saltzman, Nitrate, non-seasalt sulfate and methane-sulfonate over the Pacific Ocean, in *Chemical Oceanography*, edited by J. P. Riley, R. Chester, and R. A. Duce, vol. 10, pp. 219–250, Academic, San Diego, Calif., 1989.

Savoie, D. L., J. M. Prospero, R. J. Larsen, F. Huang, M. Izaguirre, T. Huang, T. H. Snowdon, L. Custals, and C. G. Sanderson, Nitrogen and sulfur species in Antarctic aerosols at Mawson, Palmer Station, and Marsh (King George Island), *J. Atmos. Chem.*, *17*, 95–122, 1993.

Savoie, D. L., J. M. Prospero, R. Arimota, and R. A. Duce, Non-sea-salt sulfate and methanesulfonate at American Samoa, *J. Geophys. Res.*, *99*, 3587–3596, 1994.

Schaug, J., J. E. Hansen, K. Nodop, B. Ottar, and J. M. Pacyna, Summary report from the chemical co-ordinating center for the third phase of EMEP, *EMEP/CC-report 3/87*, The Norw. Inst. for Air Res., Lillestrom, 1987.

Shaw, R. W., and R. J. Paur, Measurements of sulfur in gases and particles during sixteen months in the Ohio River Valley, *Atmos. Environ.*, *17*, 1431–1438, 1983.

Taylor, K. E., and J. E. Penner, Response of the climate system to atmospheric aerosols and greenhouse gases, *Nature*, *369*, 734–737, 1994.

Thornton, D. C., A. R. Bandy, B. W. Blomquist, D. D. Davis, and R. W. Talbot, Sulfur dioxide as a source of condensation nuclei in the upper troposphere of the Pacific Ocean, *J. Geophys. Res.*, *101*, 1883–1890, 1996.

Thornton, D. C., A. R. Bandy, B. W. Blomquist, R. W. Talbot, and J. E. Dibb, Transport of sulfur dioxide from the Asian Pacific Rim to the North Pacific troposphere, *J. Geophys. Res.*, *102*, 28,489–28,500, 1997.

Thornton, D. C., A. R. Bandy, B. W. Blomquist, A. R. Driedger, and T. P. Wade, Sulfur dioxide distribution over the Pacific Ocean 1991–1996, *J. Geophys. Res.*, *104*, 5845–5854, 1999.

Tremblay, A., and H. Leighton, A three-dimensional cloud chemistry model, *J. Clim. Appl. Meteorol.*, *25*, 652–671, 1986.

Tremmel, H. G., W. Junkermann, and F. Slemr, Distribution of organic hydroperoxides during aircraft measurements over the northeastern United States, *J. Geophys. Res.*, *99*, 5295–5307, 1994.

Twomey, S., Influence of pollution on the short-wave albedo of clouds, *J. Atmos. Sci.*, *34*, 1149–1152, 1977.

Venkatram, A., P. K. Karamchandani, and P. K. Misra, Testing a comprehensive acid deposition model, *Atmos. Environ.*, *22*, 737–747, 1988.

Wesely, M. L., Parameterization of surface resistances to gaseous dry deposition in regional-scale numerical models, *Atmos. Environ.*, *23*, 1293–1304, 1989.

Wilson, M. F., and A. Henderson-Sellers, A global archive of land cover and soils data for use in general circulation models, *J. Clim.*, *5*, 119–143, 1985.

Yin, F., D. Grosjean, R. C. Flagan, and J. H. Seinfeld, Photooxidation of dimethyl sulfide and dimethyl disulfide, II, Mechanism evaluation, *J. Atmos. Chem.*, *11*, 365–399, 1990a.

Yin, F., D. Grosjean, and J. H. Seinfeld, Photooxidation of dimethyl sulfide and dimethyl disulfide, I, Mechanism development, *J. Atmos. Chem.*, *11*, 309–364, 1990b.

Zhang, G. J., and N. A. McFarlane, Sensitivity of climate simulations to the parameterization of cumulus convection in the Canadian Climate Centre general circulation model., *Atmos. Ocean*, *33*, 407—446, 1995.

M. C. Barth, J. T. Kiehl, and P. J. Rasch, National Center for Atmospheric Research, P.O. Box 3000, Boulder, CO 80307. (barthm@ucar.edu)

C. M. Benkovitz and S. E. Schwartz, Brookhaven National Laboratory, Upton, NY 11973.

(Received December 21, 1998; revised July 16, 1999; accepted July 21, 1999.)